On the Free Vibration Behavior of Cylindrical Shell Structures

by

Burak Ustundag

B.S., Mechanical Engineering
Turkish Naval Academy, 2006

Submitted to the Department of Mechanical Engineering
in Partial Fulfillment of the Requirements for the Degree of

Master of Science

at the

Massachusetts Institute of Technology

June 2011

Signature of Author: _____
Department of Mechanical Engineering
May 6, 2011

Certified by: _____
Klaus-Jürgen Bathe
Professor of Mechanical Engineering
Thesis Supervisor

Accepted by: _____
David E. Hardt
Ralph E. and Eloise F. Cross Professor of Mechanical Engineering
Chairman, Department Committee on Graduate Students

On the Free Vibration Behavior of Cylindrical Shell Structures

by

Burak Ustundag

Submitted to the Department of Mechanical Engineering
on May 6, 2011 in Partial Fulfillment of the Requirements for
the Degree of Master of Science in
Mechanical Engineering

Abstract

Shell structures, especially cylindrical shells, are widely used in aerospace and naval architectural industries. Submarine hulls and aircraft bodies can be idealized as cylindrical shell structures. The study of vibrations of cylindrical shells is an important aspect in the successful applications of the cylindrical shells.

The free vibration characteristics of a submarine hull have an important influence on the noise signature of the submarine. That makes the free vibration problem of the submarine hull a particular interest for the submarine community. The natural frequencies of cylindrical shells are clustered in a very narrow band and they are thus more prone to becoming involved in resonant vibrations. The determination and control of these frequencies is significant to manage the acoustic signature of the submarine.

This thesis focuses on the free vibration characteristics of stiffened and unstiffened cylindrical shells. The analysis is carried out mainly in two parts. First, the unstiffened cylindrical shell is modeled and the free vibration problem is analyzed as the shell thickness decreases. Then the cylindrical shell is stiffened with ring stiffeners and the free vibration problem of the stiffened cylindrical shell is studied.

The vibration modes of the unstiffened cylindrical shell are studied for four shells with different thicknesses. Initial tensile and compressive membrane stresses are applied separately to the shells to study the effect of the initial stresses on the free vibration modes.

The vibration modes of the stiffened cylindrical shell are studied in two steps. First, the influence of the positions of two ring stiffeners on the fundamental frequencies is studied; second, the free vibration modes of the stiffened cylindrical shell are studied. Two cylindrical shells with different thicknesses are used and they are stiffened with different numbers of ring stiffeners, which are uniformly distributed along the longitudinal axis of the shell.

The results are compared with available analytical results and finite element solutions of similar problems from the literature.

Thesis Supervisor: Klaus-Jürgen Bathe

Title: Professor of Mechanical Engineering

This page intentionally left blank.

“Science is the most genuine guide in life.”

“Hayatta en hakiki mürşit ilimdir.”

Mustafa Kemal ATATÜRK

This page intentionally left blank.

Acknowledgements

I want to express my deep gratitude to Prof. Klaus-Jürgen Bathe for his continuous interest, encouragement and guidance throughout my study at MIT. He was tremendously patient with me during my times of learning, and with his endless knowledge of finite element methods and enthusiasm for teaching he is an excellent advisor; working with him has been a challenging and enjoyable experience. He is an inspiration to all his students and I'm very proud to have worked with him.

I am also very grateful to my colleagues in the Finite Element Research Group at MIT, for their friendly support and assistance. In particular, I want to thank my friends Asst. Prof. Zafer Kazancı and Daniel Payen, for their valuable discussions throughout my study.

I would like to thank ADINA R&D, Inc. for allowing me to use their proprietary finite element software ADINA for my research work.

I am also thankful to the Turkish Navy for providing me a unique education and supporting my study at MIT. I am very proud to be a member of this family.

I also would like to express my sincere appreciation to my wife Şennur, my parents Melek and Kenan, and my brother Salih for their unconditional support in every aspect of my life.

Finally, I would like to express my deepest gratitude and special thanks to my beloved spouse Şennur Aşuk Üstündağ. I thank her for her unconditional love and support, and for all the sacrifices she made just to be with me throughout my education at MIT. With her presence, everything is just easier.

This page intentionally left blank.

Table of Contents

List of Figures

List of Tables

Nomenclature

A	area
$\boldsymbol{B}$	the strain-displacement matrix
$\boldsymbol{B}_L, \boldsymbol{B}_{NL}$	the linear and nonlinear strain-displacement matrices, respectively
b_f	width of the flange of the T cross-section
$\boldsymbol{C}$	stress-strain material matrix
D	bending rigidity of the shell, $D = \frac{Et^3}{12(1-\nu^2)}$
E	Young's modulus
${}_0e_{ij}$	linear strain increment in the Lagrangian formulation
$\boldsymbol{f}^B$	vector of body forces (force/unit volume)
f_i^B	i^{th} component of the body force vector
$\boldsymbol{f}^{S_f}$	vector of surface tractions (force/unit area)
$f_i^{S_f}$	i^{th} component of the surface traction vector
$\boldsymbol{H}$	the displacement interpolation matrix
$\boldsymbol{H}^S$	the surface interpolation matrix
h_w	height of the web of the T cross-section
I_T, I_R	moment of inertia of T cross-section and rectangular cross-section, respectively
$\boldsymbol{K}$	the stiffness matrix
${}_0^t\boldsymbol{K_L}, {}_0^t\boldsymbol{K_{NL}}$	the linear strain incremental and the nonlinear strain incremental stiffness matrices, respectively
L	half of the length of the cylindrical shell
l_x	distance between two ring stiffeners
$\boldsymbol{M}$	the mass matrix
m	the number of longitudinal "half" waves
n_j	j^{th} component of the unit normal vector to the surface of the body
n	the number of circumferential "full" waves
$\boldsymbol{R}$	the load vector
R	radius of the hemisphere and the cylinder

$\boldsymbol{R}_C$	vector of the concentrated loads
S	the total surface area of the body
S_f	the surface area of the body on which the forces are applied
S_u	the surface area of the body on which the displacements are prescribed
${}_0^tS_{ij}$	components of the Piola-Kirchhoff stresses
t	thickness of the shell, hull thickness of the submarine
t_f, t_w	thickness of the flange and web of the T cross-section, respectively
$\boldsymbol{U}, \widehat{\boldsymbol{U}}$	vector of the displacements
$\boldsymbol{U}^{S_u}$	vector of the prescribed displacements on S_u
u_i	i^{th} component of the displacement vector
$\bar{u}_i$	i^{th} component of the virtual displacement vector; the overbar denotes the virtual quantities
U, V, W	displacement components in X, Y, Z directions, respectively
V	volume of the body
z	coordinate measured in the longitudinal direction from the center of the cylinder

Greek symbols

δ	when used in front of any quantity it states that the quantity is virtual (e.g. δu_i: components of virtual displacements)
$\boldsymbol{\epsilon}$	strain tensor
$\epsilon_{ij}, \gamma_{ij}$	components of the strain tensor
${}_0^t\epsilon_{ij}$	components of the Green-Lagrange strains
${}_0\eta_{ij}$	nonlinear strain increment in the Lagrangian formulation
ν	Poisson's ratio
ρ	the mass density
$\boldsymbol{\tau}$	stress tensor
$\boldsymbol{\tau^I}$	tensor of given initial stresses
τ_{ij}	components of the stress tensor
Φ	the matrix which contains the mode shapes (eigenvectors)

$\boldsymbol{\phi}$	the mode shape vector in the frequency analysis (eigenvector)
$\boldsymbol{\Omega^2}$	the matrix which contains the eigenvalues (square of the frequencies)
ω, ω^2	natural frequency, eigenvalue of the frequency equation, respectively

Notation

$\boldsymbol{A}$	matrices are represented as boldface letters.
$\boldsymbol{A}^T$	T-letter at the right superscript denotes the transpose of the matrix.
A_{ij}	components of the $\boldsymbol{A}$ matrix. Right subscripts denote the components where $i, j = X, Y, Z$ or 1,2,3
$A_{ij,j}$	$= \frac{\partial A_{ij}}{\partial x_j}$. Comma notation states the derivatives.
A_{ii}	$= A_{11} + A_{22} + A_{33}$ where $i = 1,2,3$. Repeating indices for the components means summation over the range of that component.
${}^{t}_{0}A_{ij}$	A is measured at time t referring to the initial configuration which is at time 0. The left superscript denotes the time at which the quantity is measured and the left subscript denotes the time of the configuration at which the measurement is referred to.
${}^{t}_{0}A_{i,j}$	$= \frac{\partial\ {}^{t}A_i}{\partial\ {}_{0}x_j}$

This page intentionally left blank.

1. Introduction

Shell structures are widely used structural components in engineering designs. Basically, a shell structure is a three-dimensional structure which is thin in one direction and long in the other two directions. Because of this geometric aspect, they are thin, light and they span over large areas. Although they are thin, they can carry applied loads effectively by means of their curvatures. They are commonly used in construction of large roofs in civil engineering, in the bodies of cars in the automobile industry, in the airplane bodies and rockets in aeronautical engineering and finally in ship/submarine hulls in naval architecture. The objective of the design is to make the shell as thin as possible in order to have a light and low cost, but a functional structure. However, shells can be extremely sensitive to imperfections and changes in the thickness and boundary conditions.

A special type of shells is the cylindrical shell. Cylindrical shells are found in many applications in the aerospace and naval construction industries. They are often used as load-bearing structures for aircrafts, rockets, submarines and missile bodies. Of course, the cylindrical shells used in those designs are stiffened to achieve better strength, stiffness and buckling characteristics. The study of vibrations of cylindrical shells is an important aspect in the successful applications of cylindrical shells.

A submarine hull can basically be idealized as a ring-stiffened cylindrical shell for the purposes of vibration analysis. The free vibration characteristics of a submarine hull have an important influence on the noise signature of the submarine. That makes the free vibration problem of the submarine hull a particular interest for the submarine community. Determination of the natural frequencies and the corresponding mode shapes of the submarine is an important problem for the acoustic signature management of the submarine. The acoustic signature is strongly influenced by hull vibrations, particularly at low to medium frequencies. On the other hand, the lower frequencies are also sensitive to a variation in external pressure or the thickness of the hull. The determination of these low frequencies is significant to manage the acoustic signature of the submarine [1].

The natural frequencies of the cylindrical shells are clustered in a very narrow band and they are thus more prone to becoming involved in resonant vibrations. To control the amplitudes

of these vibrations, it is necessary to know the distribution of the natural frequencies, since this allows us to design the cylindrical shell structures from the viewpoint of optimum vibration control [2].

The objective of this thesis is to study the free vibration characteristics of cylindrical shells with different thicknesses. The analysis is carried out mainly in two parts. First, the unstiffened cylindrical shell is modeled and the free vibration problem is analyzed. Then the cylindrical shell is stiffened with ring stiffeners and the free vibration problem of the stiffened cylindrical shell is studied. The results are compared with the available analytical results and the finite element solutions of similar problems from the literature.

A brief explanation on the finite element formulation regarding the subjects covered in this thesis is presented in Chapter 2. The process of the finite element analysis is summarized and the finite element equations for the static and the free vibration analyses are derived. Descriptions of the elements used in the finite element model are also presented.

Chapter 3 includes information on the finite element model analyzed. The geometry and the material properties are presented. Mesh density and element type study explains how the finite element model is meshed.

The study on the free vibration characteristics of the unstiffened cylindrical shells is presented in Chapter 4. The variation of the frequencies and of the corresponding mode shapes is studied as the thickness of the shell decreases. Initial tensile and compressive membrane stresses are applied on the cylindrical shell and the effect of the initial stresses on the free vibration modes is investigated. The effect of the initial stresses on the rigid body modes of the cylindrical shell is an important conclusion of this study. Chapelle and Bathe [3] have discussed the same problem for the clamped cylindrical shell. The results obtained in this thesis are consistent with the results of the study presented in [3]. The analytical solution of the free vibration problem of an unstiffened, unstressed cylindrical shell is obtained and compared with the finite element solution. The finite element solution is quite consistent with the analytical solution of the problem.

The study of the free vibration characteristics of the ring-stiffened cylindrical shells is presented in Chapter 5. The variation of the fundamental frequencies with the positions of the ring stiffeners and the variation of the frequencies with the number of uniformly distributed ring stiffeners are studied in two parts. To analyze the effect of the positions of the ring stiffeners, the cylindrical shell is stiffened with two ring stiffeners and the positions of the ring stiffeners are changed in turn. The results are compared with the study of Loy and Lam [4]. That comparison gives an insight on how the assumptions made through the analysis affect the results. The variation of the frequencies with the number of uniformly distributed ring stiffeners is studied next. The effect of the ring stiffeners on the vibration modes is investigated. The analytical solution of the free vibration problem of the ring-stiffened cylindrical shell is solved for the cylindrical shell stiffened with three stiffeners. The finite element solution is compared with the analytical solution for the cylindrical shell stiffened with three stiffeners.

Finally in Appendix A, the solution of the free vibration problem of a truss element is presented. The objective of this presentation is to give an insight on the effect of the initial stresses on the rigid body modes of the structures. The reason to choose the truss element is to study the problem in the simplest way possible and use the results to understand the response of more complex structures such as the one studied in Chapter 4. The results warrant important conclusions on the effect of the initial stresses on the rigid body modes of structures.

All finite element solutions presented in this thesis are obtained using ADINA.

2. Finite Element Formulation

2.1 The Process of the Finite Element Analysis

In the finite element analysis, the solution of the mathematical model of a physical structure is numerically obtained using finite element procedures [3]. The physical problem consists of an actual structure or phenomenon with known material properties, subjected to certain loading and boundary conditions. The mathematical model of this physical problem is established using some assumptions. The finite element analysis solves this mathematical model and allows the analyst to predict the response of the structure without building the structure. Since the finite element analysis deals only with the mathematical model of the physical structure, it is very important to use a mathematical model that represents the physical structure adequately. It is obvious that the finite element analysis can predict only what is considered in the mathematical model. We cannot expect any more information from the solution than what is contained in the mathematical model. Hence, it is crucial for the analyst to use an appropriate mathematical model. The choice of the mathematical model determines the insight into the physical problem that we can obtain by the analysis [5].

Solution of the mathematical model by the finite element analysis should be interpreted by the analyst. According to the results, refinements in the mathematical model may be made and that will lead to additional finite element solutions. The choice of the mathematical model is an important part of the analysis. The mathematical model should be reliable and effective in predicting the solution. An effective mathematical model is the one which yields the required solution to a sufficient accuracy and at least cost. A mathematical model is reliable, if the required solution is known to be predicted within a selected level of accuracy measured on the response of the very comprehensive mathematical model [5].

The interpretation of the results of the finite element solution may lead the analyst to make a refinement on the mathematical model. That is, the higher-order mathematical models should be considered in the analysis. For example, a beam structure may first be analyzed using Bernoulli beam theory, then Timoshenko beam theory, then two-dimensional plane stress theory,

and finally using a three-dimensional continuum model. Such a sequence of models is referred to as a hierarchy of models and the analysis will include ever more complex response effects [5].

The process of the finite element analysis is basically summarized as the choice of the appropriate mathematical model, solution of the mathematical model with the finite element analysis, and the evaluation of these results.

2.2 Derivation of the Finite Element Equations

The aim of the analyst is to calculate the response of the structure considered in the problem. We will consider a body, arbitrarily taken from the universe, to state the problem. The governing differential equations for the equilibrium of this body lead us to the principle of virtual displacements. The principle of virtual displacements (also known as the principle of virtual work) is the basis of the displacement-based finite element solution [5].

The problem should be solved for a general three-dimensional body which is presented in Figure 2.1. The body is located in the fixed coordinate system X, Y, Z. The body surface area is composed of two areas such that $S_u \cap S_f = 0$ and $S_u \cup S_f = S$. The body is supported on the area S_u with prescribed displacements $\boldsymbol{U}^{S_u}$ and is subjected to surface tractions $\boldsymbol{f}^{S_f}$ (forces per unit surface area) on the surface area S_f. The body is also subjected to externally applied body forces $\boldsymbol{f}^B$ (forces per unit volume) and concentrated loads $\boldsymbol{R}_C$ at certain points.

The solution of the problem should give us the displacements and the corresponding strains and stresses. The displacements of the body are measured in the fixed coordinate system presented in Figure 2.1 and defined as

$$\boldsymbol{U}(X,Y,Z) = [U \quad V \quad W]^T \tag{2.1}$$

The strains corresponding to $\boldsymbol{U}$ are

$$\boldsymbol{\epsilon} = [\epsilon_{XX} \quad \epsilon_{YY} \quad \epsilon_{ZZ} \quad \gamma_{XY} \quad \gamma_{YZ} \quad \gamma_{ZX}]^T \tag{2.2}$$

where

$$\epsilon_{XX} = \frac{\partial U}{\partial X}; \quad \epsilon_{YY} = \frac{\partial V}{\partial Y}; \quad \epsilon_{zz} = \frac{\partial W}{\partial Z}$$

$$\gamma_{XY} = \frac{\partial U}{\partial Y} + \frac{\partial V}{\partial X}; \quad \gamma_{YZ} = \frac{\partial V}{\partial Z} + \frac{\partial W}{\partial Y}; \quad \gamma_{ZX} = \frac{\partial W}{\partial X} + \frac{\partial U}{\partial Z} \tag{2.3}$$

The stresses corresponding to $\boldsymbol{\epsilon}$ are

$$\boldsymbol{\tau} = [\tau_{XX} \quad \tau_{YY} \quad \tau_{ZZ} \quad \tau_{XY} \quad \tau_{YZ} \quad \tau_{ZX}]^T \tag{2.4}$$

where the stress is defined as

$$\boldsymbol{\tau} = \boldsymbol{C\epsilon} + \boldsymbol{\tau^I} \tag{2.5}$$

In (2.5) $\boldsymbol{C}$ is the stress strain material matrix and $\boldsymbol{\tau^I}$ denotes given initial stresses.

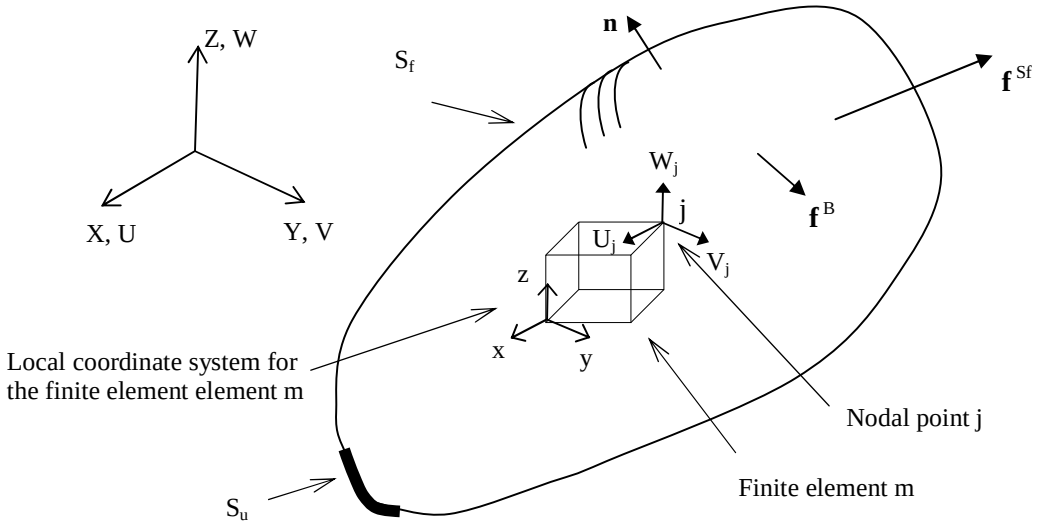

Figure 2.1: General three-dimensional body.

In summary, we have a problem to analyze with the given geometry of the body, the applied loads, the boundary conditions, the material stress-strain law and the initial stresses in the

body. The expected result is the response of the body. That is, the displacements of the body and the corresponding strains and stresses.

2.2.1 The Principle of Virtual Displacements

The principle of virtual displacements is the basis of the finite element formulation. This principle states that the equilibrium of the body requires that for any compatible virtual displacements imposed on the body in its state of equilibrium, the total internal virtual work is equal to the total external virtual work [5].

The derivation of the principle of virtual displacements is presented in details in Chapter 4 of [5] and the same procedure is adopted in this section. Here, very brief information on the derivation is presented to give an insight on the finite element formulation.

The analysis of the elastic body described here requires consideration of three fundamental principles. These principles, also referred to as the three aspects of solid mechanics problems, are equilibrium, compatibility and the stress-strain law [6]. They can be summarized as the following:

- *Equilibrium*: The equilibrium equations must be satisfied throughout the body.
- *Compatibility*: The displacement field must be continuous and satisfy the displacement boundary conditions.
- *Stress-strain law*: Material properties (constitutive relations) must comply with the known behavior of the material considered.

The principle of virtual displacements must satisfy the governing equations for the body and is derived from those equations. The governing equations of the body are the equilibrium equation along with the static and the kinematic boundary conditions [6]. The governing differential equations for the body are

$$\tau_{ij,j} + f_i^B = 0 \qquad \text{throughout the body} \tag{2.6}$$

with the static (force) boundary conditions

$$\tau_{ij} n_j = f_i^{S_f} \qquad \text{on } S_f \tag{2.7}$$

and the kinematic (displacement) boundary conditions

$$u_i = u_i^{S_u} \qquad \text{on } S_u \tag{2.8}$$

where n_j are the components of the unit normal vector to the surface S of the body.

Now consider any arbitrarily chosen, continuous displacements $\bar{u}_i$ satisfying the displacement boundary conditions on S_u. Those displacements are called the virtual displacements. Multiply (2.6) with the virtual displacements and integrate over the body. Therefore we have

$$\int_V (\tau_{ij,j} + f_i^B)\, \bar{u}_i dV = 0 \tag{2.9}$$

Since $\bar{u}_i$ are arbitrary, (2.9) can be satisfied if the quantity in the parenthesis is zero. Hence (2.9) is equivalent to (2.6). Performing the integral in (2.9) by integration of parts and using (2.7) and (2.8) through the calculation we obtain

$$\int_V \tau_{ij} \bar{\epsilon}_{ij} dV = \int_V f_i^B \bar{u}_i dV + \int_{S_f} f_i^{S_f} \bar{u}_i^{S_f} dS^f + \sum_n \bar{u}_i^n R_{Ci}^n \tag{2.10}$$

as the principle of virtual displacements in tensor notation for the three-dimensional body. In (2.10), the term " $\sum_n \bar{u}_i^n R_{Ci}^n$ " represents the summation of the corresponding components of *n* concentrated forces. The left-hand side of (2.10) is the internal virtual work and the right-hand side is the external virtual work. In matrix notation the principle of virtual displacements is expressed as

$$\int_V \bar{\boldsymbol{\epsilon}}^T \boldsymbol{\tau} dV = \int_V \bar{\boldsymbol{U}}^T \boldsymbol{f}^B dV + \int_{S_f} \bar{\boldsymbol{U}}^{S_f^T} \boldsymbol{f}^{S_f} dS^f + \sum_n \bar{\boldsymbol{U}}^{n^T} \boldsymbol{R}_C^n \tag{2.11}$$

It is important to note that, when the principle of virtual displacements is satisfied all three fundamental requirements of mechanics are satisfied [5]:

- *Equilibrium* is satisfied because (2.10) is derived from the governing equilibrium equations (2.6-2.8) of the body.

- *Compatibility* holds because the displacement field is continuous and satisfies the displacement boundary conditions.

- *Stress-strain law* holds because the stresses in (2.10) are calculated using constitutive equations from the strains.

2.2.2 The Finite Element Equations

Now that the principle of virtual displacements has been presented, we can derive the governing finite element equations. In the finite element analysis, the body is approximated as an assemblage of discrete finite elements. Those elements are interconnected at nodal points on the element boundaries. The displacements measured in the local coordinate system of each element are assumed to be a function of the displacements at the nodes of the element. Therefore, for each element, first the displacements at the nodes are calculated and then those displacements are interpolated to obtain the displacement within the element. For element *m* we have

$$\boldsymbol{u}^{(m)} = \boldsymbol{H}^{(m)}(x, y, z)\widehat{\boldsymbol{U}} \tag{2.12}$$

where $\boldsymbol{H}^{(m)}$ is the displacement interpolation matrix, the superscript *m* denotes element *m* and $\widehat{\boldsymbol{U}}$ is a vector of global displacement components at all nodal points. So $\widehat{\boldsymbol{U}}$ is a vector of dimension 3N where N is the total number of the nodes of the element.

$$\widehat{\boldsymbol{U}} = [U_1 \quad V_1 \quad W_1 \quad \dots \quad U_N \quad V_N \quad W_N]^T \tag{2.13}$$

The displacement interpolation matrix is evaluated particularly for the element type and the evaluation depends on the geometry and the number of the nodes of the element.

From the displacement assumption in (2.12) corresponding strains are obtained as

$$\boldsymbol{\epsilon}^{(m)}(x, y, z) = \boldsymbol{B}^{(m)}(x, y, z)\widehat{\boldsymbol{U}} \tag{2.14}$$

where $\boldsymbol{B}^{(m)}$ is the strain-displacement matrix. The rows of $\boldsymbol{B}^{(m)}$ are obtained by using the relations in (2.3) and differentiating the rows of $\boldsymbol{H}^{(m)}$.

The stresses in the element are obtained by using the element strains and the element initial stresses. The stresses are defined as

$$\boldsymbol{\tau}^{(m)} = \boldsymbol{C}^{(m)}\boldsymbol{\epsilon}^{(m)} + \boldsymbol{\tau}^{\boldsymbol{I}(m)} \tag{2.15}$$

where $\boldsymbol{C}^{(m)}$ is the elasticity matrix of the element *m* and $\boldsymbol{\tau}^{\boldsymbol{I}(m)}$ are the given element initial stresses.

In the finite element analysis, the body is assumed as an assemblage of discrete finite elements. To derive the governing finite elements equations for the body, let's rewrite (2.11) as a sum of integrations over the volumes and areas of all finite elements:

$$\sum_m \int_{V^{(m)}} \bar{\boldsymbol{\epsilon}}^{(m)T}\boldsymbol{\tau}^{(m)} dV^{(m)} = \sum_m \int_{V^{(m)}} \bar{\boldsymbol{u}}^{(m)T}\boldsymbol{f}^{B(m)} dV^{(m)} + \sum_m \int_{S_1^{(m)},\dots,S_q^{(m)}} \bar{\boldsymbol{u}}^{S_{(m)}^T}\boldsymbol{f}^{S_{(m)}} dS^{(m)} + \sum_n \bar{\boldsymbol{u}}^{n^T}\boldsymbol{R}_C^n \tag{2.16}$$

where $S_1^{(m)}, \ldots, S_q^{(m)}$ denotes the element surfaces that are part of the body surface S. We need to obtain the virtual displacements and strains in finite element formulation to be used in (2.16). The relations given in (2.12) and (2.14) are for the element displacements and strains. However, the same relations hold for the virtual displacements and strains. Using those relations we have

$$\bar{\boldsymbol{u}}^{(m)} = \boldsymbol{H}^{(m)}(x,y,z)\bar{\bar{\boldsymbol{U}}}; \qquad \bar{\boldsymbol{\epsilon}}^{(m)}(x,y,z) = \boldsymbol{B}^{(m)}(x,y,z)\bar{\bar{\boldsymbol{U}}} \tag{2.17}$$

Substituting (2.12, 2.14, 2.15 and 2.17) in (2.16) we obtain

$$\begin{aligned} \bar{\bar{\boldsymbol{U}}}^T \left[\sum_m \int_{V^{(m)}} \boldsymbol{B}^{(m)T}\boldsymbol{C}^{(m)}\boldsymbol{B}^{(m)} dV^{(m)}\right]\hat{\boldsymbol{U}} \\ = \bar{\bar{\boldsymbol{U}}}^T \left[\left\{\sum_m \int_{V^{(m)}} \boldsymbol{H}^{(m)T}\boldsymbol{f}^{B(m)} dV^{(m)}\right\} + \left\{\sum_m \int_{S_1^{(m)},\ldots,S_q^{(m)}} \boldsymbol{H}^{S(m)T}\boldsymbol{f}^{S_{(m)}} dS^{(m)}\right\} \right. \\ \left. - \left\{\sum_m \int_{V^{(m)}} \boldsymbol{B}^{(m)T}\boldsymbol{\tau}^{I(m)} dV^{(m)}\right\} + \boldsymbol{R}_C\right] \end{aligned} \tag{2.18}$$

where the surface interpolation matrices $\boldsymbol{H}^{S(m)}$ are obtained from the displacement interpolation matrices (2.12) by substituting the appropriate element surface coordinates and $\boldsymbol{R}_C$ is a vector of concentrated loads applied to the nodes of the element assemblage.

In order to obtain the equations for the unknown nodal point displacements, the principle of virtual displacement (2.18) is applied N times by imposing unit virtual displacements in turn for all components of $\bar{\bar{\boldsymbol{U}}}$. Therefore we obtain

$$\boldsymbol{K}\boldsymbol{U} = \boldsymbol{R} \tag{2.19}$$

where $\boldsymbol{K}$ is the stiffness matrix and

$$\boldsymbol{R} = \boldsymbol{R}_B + \boldsymbol{R}_S - \boldsymbol{R}_I + \boldsymbol{R}_C \tag{2.20}$$

From now on, for simplicity $\widehat{\boldsymbol{U}}$ will be replaced by $\boldsymbol{U}$. Using the relation between (2.18) and (2.19), the stiffness matrix of the element assemblage is

$$\boldsymbol{K} = \sum_m \boldsymbol{K}^{(m)} = \sum_m \int_{V^{(m)}} \boldsymbol{B}^{(m)T} \boldsymbol{C}^{(m)} \boldsymbol{B}^{(m)} dV^{(m)} \tag{2.21}$$

The load vector $\boldsymbol{R}$ includes the effect of the element body forces,

$$\boldsymbol{R}_B = \sum_m \boldsymbol{R}_B{}^{(m)} = \sum_m \int_{V^{(m)}} \boldsymbol{H}^{(m)T} \boldsymbol{f}^{B(m)} dV^{(m)} \tag{2.22}$$

the effect of the element surface forces

$$\boldsymbol{R}_S = \sum_m \boldsymbol{R}_S{}^{(m)} = \sum_m \int_{S_1^{(m)},\ldots,S_q^{(m)}} \boldsymbol{H}^{S(m)T} \boldsymbol{f}^{S_{(m)}} dS^{(m)} \tag{2.23}$$

the effect of the element initial stresses

$$\boldsymbol{R}_I = \sum_m \boldsymbol{R}_I{}^{(m)} = \sum_m \int_{V^{(m)}} \boldsymbol{B}^{(m)T} \boldsymbol{\tau}^{\boldsymbol{I}(m)} dV^{(m)} \tag{2.24}$$

and the nodal concentrated loads $\boldsymbol{R}_C$.

Equation (2.19) states the static equilibrium of the element assemblage. For the solution of the dynamic problems, inertia forces need to be considered in the equilibrium equations. The element inertia forces can be included as part of the body forces. So the effect of the total body forces is

$$\boldsymbol{R}_B = \sum_m \int_{V^{(m)}} \boldsymbol{H}^{(m)T}\left[\boldsymbol{f}^{B(m)} - \rho^{(m)}\boldsymbol{H}^{(m)}\ddot{\boldsymbol{U}}\right] dV^{(m)} \tag{2.25}$$

where $\boldsymbol{f}^{B(m)}$ no longer includes inertia forces, $\ddot{\boldsymbol{U}}$ is a vector of the nodal point accelerations and $\rho^{(m)}$ is the mass density of element *m*. The nodal point accelerations are the second time derivatives of $\boldsymbol{U}$ and are approximated in the same way as the displacements. For the dynamic equilibrium we have

$$\boldsymbol{M}\ddot{\boldsymbol{U}}(t) + \boldsymbol{K}\boldsymbol{U}(t) = \boldsymbol{R}(t) \tag{2.26}$$

where the mass matrix of the structure is defined as

$$\boldsymbol{M} = \sum_m \boldsymbol{M}^{(m)} = \sum_m \int_{V^{(m)}} \rho^{(m)}\boldsymbol{H}^{(m)T}\boldsymbol{H}^{(m)} dV^{(m)} \tag{2.27}$$

2.2.3 The Finite Element Formulation of the Free Vibration Problem

The free vibration problem of structures is a dynamic problem and the dynamic equilibrium equation (2.26) should be considered to derive the solution. The free vibration term states that there are no externally applied loads on the structure and the structure is vibrating freely. Hence the load vector $\boldsymbol{R}$ is zero in (2.26). The equilibrium equation of the body under free vibration conditions is

$$\boldsymbol{M}\ddot{\boldsymbol{U}} + \boldsymbol{K}\boldsymbol{U} = \boldsymbol{0} \tag{2.28}$$

The solution to (2.28) can be postulated in the form

$$\boldsymbol{U} = \boldsymbol{\phi}\, \sin(\omega t) \tag{2.29}$$

Substituting (2.29) in (2.28) we obtain the eigenproblem from which the frequencies and the corresponding mode shapes can be determined.

$$\boldsymbol{K\phi} = \omega^2 \boldsymbol{M\phi} \tag{2.30}$$

where ω is the frequency of the free vibration and $\boldsymbol{\phi}$ is the corresponding mode shape vector. The eigenproblem in (2.30) yields *n* eigensolutions. The solution contains an eigenvalue which is the square of the frequency of the free vibration (radians/sec) and an eigenvector which is the corresponding mode shape. The following two new matrices are defined to store the *n* eigensolutions:

$$\boldsymbol{\Phi} = [\boldsymbol{\phi}_1, \boldsymbol{\phi}_2, \dots\dots, \boldsymbol{\phi}_n]; \qquad \boldsymbol{\Omega^2} = \begin{bmatrix} \omega_1^2 & & & \\ & \omega_2^2 & & \\ & & \ddots & \\ & & & \omega_n^2 \end{bmatrix} \tag{2.31}$$

Using the matrices in (2.31), we can write *n* solutions to (2.30) as

$$\boldsymbol{K\Phi} = \boldsymbol{M\Phi\Omega^2} \tag{2.32}$$

The solution to (2.32) gives the natural frequencies and the corresponding mode shapes of the structure.

2.3 Element Descriptions and Assumptions

Free vibrations of stiffened and unstiffened cylindrical shells are studied in this thesis. In the finite element model, the shell surface is modeled with 9-node shell elements and the ring stiffeners are modeled with 3-node iso-beam elements. Shell elements are attached to beam elements using rigid links to model the stiffened cylindrical shell. The details regarding the modeling process are presented in relevant sections. In this section, brief descriptions of the elements are presented.

2.3.1 Iso-beam Elements

Iso-beam elements are used to model the ring stiffeners in the stiffened cylindrical shell model. General consideration for the iso-beam elements are listed in the following [7]:

- The iso-beam elements can be employed as plane stress 2-D beam with three degrees of freedom per node, plane strain 2-D beam with three degrees of freedom per node,

axisymmetric shell with three degrees of freedom per node and general 3-D beam with six degrees of freedom per node.

- The cross-sectional areas of each of these elements are assumed to be rectangular. The two-dimensional and three-dimensional beam elements can only be assigned a cross-section with constant area. The axisymmetric shell element can be assigned a varying thickness.

- The elements can be employed with 2, 3 or 4 nodes. The 3 and 4-node elements can be curved, but it should be noted that the element nodes must initially lie in one plane (which defines the r-s plane). The iso-beams elements are presented in Figure 2.2.

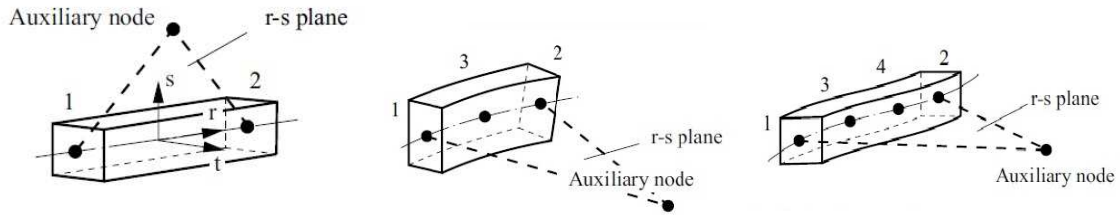

(a) 2-node iso-beam (b) 3-node iso-beam (c) 4-node iso-beam

Figure 2.2: Iso-beam elements [7].

The iso-beam elements are primarily used to model curved beams, stiffeners to shells, beams in large displacements and axisymmetric shells under axisymmetric loading. Since iso-beam elements are able to model curved beams, they are chosen to model the ring stiffeners in this study.

The formulation of the iso-beam elements is derived using the principle of virtual displacements and a detailed derivation can be found in Chapter 5 of [5]. The curved beam elements are formulated as the straight beams. However, as a result of the displacement-based formulation, the beam element displays shear and membrane locking which causes the element to be very stiff and useless. So a mixed interpolation is used to overcome the shear and membrane locking effects and obtain efficient beam elements.

The basic kinematic assumption in the formulation of the element is that plane sections which are originally orthogonal to the centerline axis remain plane under deformation but not

necessarily orthogonal to this axis. This assumption is also referred as the Timoshenko beam theory [8]. A schematic representation of the kinematic assumption is presented in Figure 2.3 which is taken from [5].

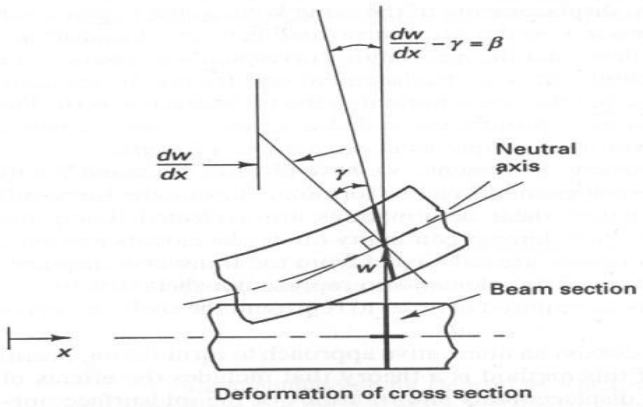

Figure 2.3: Beam deformation assumptions [5].

2.3.2 Shells Elements

Shell elements are used to model the surface of the cylindrical shell in the finite element model. The shell element is a 4 to 32-node isoparametric element that can be employed to model thick and thin general shell structures [7].

There are two basic assumptions in the formulation of the shell elements. The state of stress in the shell corresponds to plane stress conditions. That is, the stress in the direction normal to the midsurface is zero. The kinematic assumption is that plane sections originally orthogonal to the midsurface remain plane under deformation but not necessarily orthogonal to the midsurface. This assumption is similar to that of the beam, and is referred to as the Reissner-Mindlin plate theory [8]. Figure 2.4 presents the kinematic assumption on a flat shell.

Either 5 or 6 degrees of freedom can be assigned at a shell midsurface node. When 5 degrees of freedom are specified, the rotational degree of freedom around the vector which is normal to the midsurface is neglected. In general, it is appropriate to specify 5 degrees of freedom except for the following cases in which 6 degrees of freedom should be used:

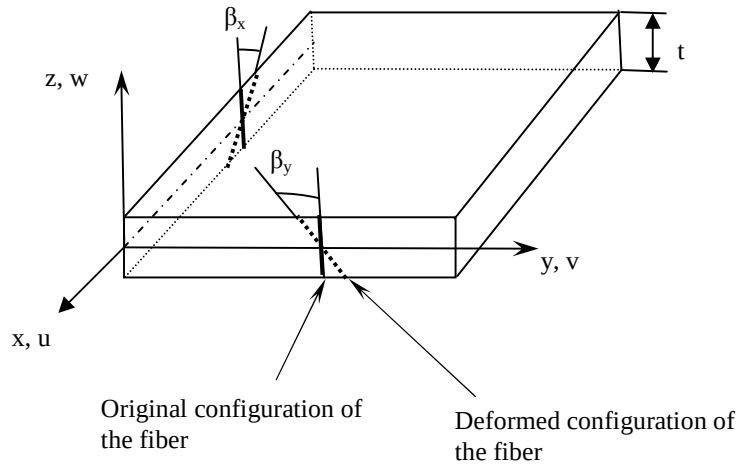

Figure 2.4: Shell deformation assumptions [5].

- Shell elements intersecting at an angle.
- Coupling of shell elements with other types of structural elements such as isoparametric beams (e.g., in the modeling of stiffened shells using shell and beam elements).
- Coupling of rigid links to the shell midsurface nodes.
- Imposing specific boundary conditions.

The formulation of the shell elements are derived using the principle of virtual displacements and a detailed derivation can be found in Chapter 5 of [5]. The approach is similar to that of the beam element. The plate element formulation is generalized to obtain the shell formulation in a similar way as the formulation of straight beam element is generalized to obtain the curved beam element. As in the case of the formulation of the beam elements, using displacement-based interpolations causes the element locking phenomenon to arise. The displacement-based elements are too stiff because the interpolation functions used are not able to represent zero (or very small) shearing and membrane strains. If the element cannot represent zero strains, but the physical situation corresponds to zero (or very small) strains, then the element becomes very stiff as its thickness decreases.

The mixed interpolation is used to overcome the element locking problem; we use the MITC (Mixed Interpolation of Tensorial Components) shell elements. For a detailed derivation and discussion of the MITC shell elements refer to [9-12] and Chapter 5 of [5]. In ADINA,

MITC elements are used to model shells. The types of shell elements are listed in Table 2.1 and some example illustrations are shown in Figure 2.5.

Table 2.1: Types of shell elements available in ADINA [7]**.**

	Number of nodes	Single layer with midsurface nodes only
Quadrilateral elements	4-node	MITC4
	8- node	MITC8
	9- node	MITC9
	16- node	MITC16
Triangular elements	3- node	MITC3
	6- node	MITC6

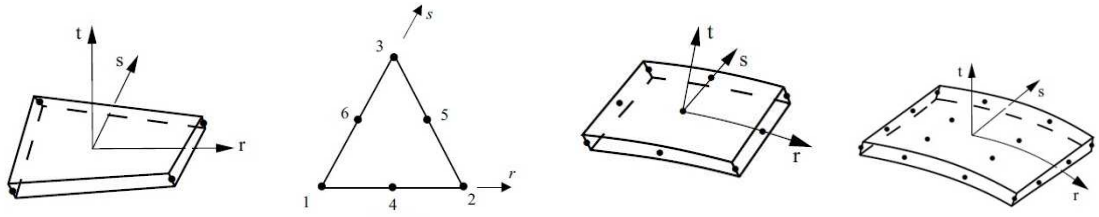

(a) MITC4 (b) MITC6 (c) MITC9 (d) MITC16

Figure 2.5: Shell elements [7]

2.3.3 Rigid Links

Rigid links are used to model the stiffened cylindrical shells in this thesis. The iso-beam elements are attached to the shell elements using rigid links in ADINA. A rigid link establishes constraint equations between the degrees of freedom of two nodes. Those nodes are called the master node and the slave node. The degrees of freedom of the master node are independent while the degrees of freedom of the slave node are dependent on those of the master node [8]. As the nodes displace, the slave node is constrained to translate and rotate such that the distance between the master node and the slave node remains constant, and that the rotations at the slave node are the same as the corresponding rotations at the master node. Usage of the rigid links in the finite element model is presented in Section 5.2.

3. Finite Element Model of the Cylindrical Shell

3.1 Geometry of the Cylindrical Shell

This thesis focuses on the free vibration analysis of stiffened and unstiffened cylindrical shells. “The cylindrical shell” term refers to a cylindrical shell which has hemispherical end closures at both ends. The dimension parameters of the hemispherical end closures and the cylindrical shell are presented separately in Figure 3.1.

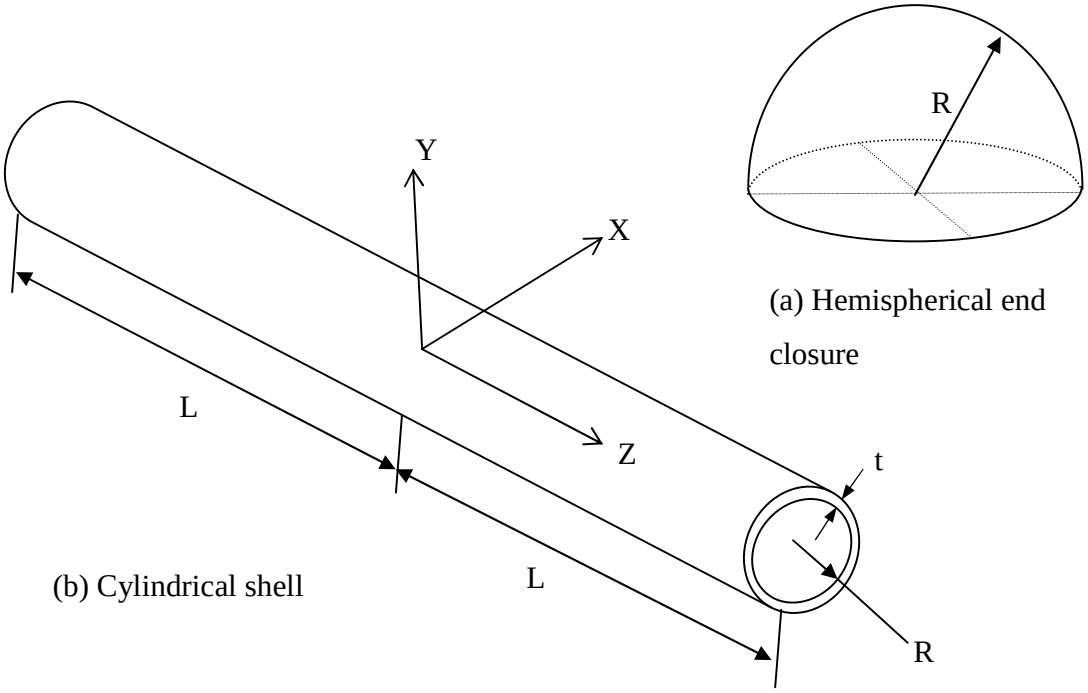

Figure 3.1: The dimension parameters of the cylindrical shell and the hemispherical end closures.

The hemispheres and the cylindrical shell have the same thickness and together compose the structure analyzed in this study. Figure 3.2 shows the cylindrical shell modeled in ADINA[1].

[1] In Figure 3.2, the model is presented with an arbitrary mesh to represent the outline of the model.

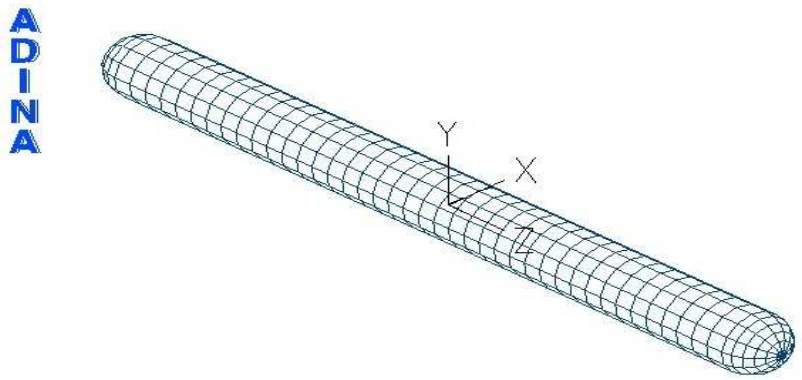

Figure 3.2: The cylindrical shell model.

The purpose of analyzing the cylindrical shell with hemispherical end closures is to relate the model to a submarine. Of course, many different types of submarines are being used by navies around the world. Using a very basic analogy, we can assume the shape of the submarine hull as a cylinder closed at both ends. Since the model dimensions are not the main concern of this study, approximate dimensions of a conventional submarine are adopted. Approximate ranges for the dimensions of a conventional submarine are listed in Table 3.1.

Table 3.1: The dimensions of the conventional submarines.

	Dimension range [m]
Length (2L)	50 ~ 60
Width (2R)	6 ~ 7
Hull thickness (t)	$18\text{x}10^{-3}$ ~ $30\text{x}10^{-3}$

Using the ranges given in Table 3.1, we obtain some geometric ratios to use as a reference for our model. The geometric ratios of the conventional submarines are

$$\frac{t}{R} \cong 10^{-2}; \quad \frac{R}{L} \cong 10^{-1} \tag{3.1}$$

The geometric ratios in (3.1) are used as reference to model the cylindrical shell in the finite element analysis. However, in the studies carried out here, the thickness of the cylindrical shell is

changed to study the free vibration behavior of the cylindrical shell. But the cylindrical shell with $t/R=10^{-2}$ is considered as the model which is closest to the reality. For this comparison only the geometry of the models is considered. The dimensions of the cylindrical shells used in the analyses are listed in Table 3.2.

Table 3.2: The dimensions of the cylindrical shells.

	Dimension [m]
Length (2L)	20
Width (2R)	2
Hull thickness	10^{-1}, 10^{-2}, 10^{-3} and 10^{-5}

The thickness of the shell is decreased up to 10^{-5} m. in the study of free vibrations of cylindrical shells. Since shells are very sensitive to thickness changes it is important to study the behavior of cylindrical shells, especially for smaller thicknesses. The advances in material science and technology are expected to result in stronger materials. In the last two decades carbon nanotubes have been an important area of research. Theoretical studies suggest that carbon nanotubes can have a Young's modulus as high as 1 TPa and yield strength close to 50 GPa. With those mechanical properties carbon nanotubes are thought of as ideal candidates for structural applications. Many studies have been carried out to develop carbon nanotube-based composites for applications in the aerospace industry, especially by NASA [13]. Structural applications of those carbon nanotube-based composites in the industry may result in very thin shell structures such as in submarines, airplanes and rockets. In the future we may need to analyze thinner shells compared to those designed now.

3.2 Material Properties of the Finite Element Model

The cylindrical shell model used in the finite element analysis is related to the model of conventional submarines. High-strength alloyed steel, particularly HY-80, is the main material for submarines. So the material properties of HY-80 steel are used in the finite element model. The material properties used in the model are listed in Table 3.3.

Table 3.3: The material properties of the model.

Material Properties	Values
Young's modulus (E)	205 GPa
Poisson's ratio (ν)	0.28
The mass density (ρ)	7,870 kg/m^3

3.3 Mesh Density and Element Type Study

Meshing is an important part of finite element analysis. In the process of analysis special attention should be given to mesh the model in the best way possible. The same model can be meshed using various element sizes and types. The aim is to find the most appropriate and efficient element type and size to do the analysis. Finding the most appropriate and efficient mesh is highly dependent on the computational resources, because as the mesh gets finer more computational resources are needed for the analysis. So the computational capability of the computer which the analyst is using is one of the main factors in order to determine the mesh density and element type. Also the formulation of the element type is an important factor to select that element type to mesh the model. Considering the type of the analysis and the physical model, an element type which will be able to represent the physical model best should be chosen. The formulation of the element type and the selection of the right elements for the analysis is a wide subject and detailed discussions can be found in [5] and [7].

The mesh density and element type study is performed using 4-node and 9-node shell elements on four different unstiffened-unstressed cylindrical shells, each having different thicknesses. The shells are meshed with 4-node and 9-node shell elements separately. The variation of the fundamental frequency with element size "h" is studied. The element size is decreased and the mesh is finer at each step. The element size is the length of the longest side of one element. At every step, the fundamental frequency is calculated and the variation of the fundamental frequency with the element size is studied for each model. The performances of the 4-node and 9-node shell elements are also compared.

The computational resources play a significant role to choose the mesh density and element type. The cost of the computation is directly related to the number of elements and nodes of the model. In order to have an idea of how those quantities vary by the element size, Table 3.4 is presented.

Table 3.4: The number of elements and nodes for different element sizes.

Element Size (h)	Element Type	Number of elements	Number of nodes
0.5	4-node shell	624	613
	9-node shell	624	2,466
0.4	4-node shell	928	914
	9-node shell	928	3,650
0.3	4-node shell	1,659	1,640
	9-node shell	1,659	6,554
0.2	4-node shell	3,608	3,577
	9-node shell	3,608	14,302
0.15	4-node shell	6,426	6,386
	9-node shell	6,426	25,538
0.12	4-node shell	10,050	9,998
	9-node shell	10,050	39,986
0.1	4-node shell	14,552	14,491
	9-node shell	14,552	57,958
0.08	4-node shell	22,752	22,611
	9-node shell	22,752	90,438
0.06	4-node shell	40,425	40,130
	9-node shell	40,425	160,514

The shell elements are studied in [9-12] and [14]. The recommended elements for the analysis of shells are 4-node, 9-node and 16-node shell elements. In this study 4-node and 9-node shell elements are compared according to their performances in calculating the fundamental frequencies of our models. As presented in Table 3.4 element size is decreased up to 0.06. The model which is meshed with this element size has 40,425 elements, 40,130 nodes when 4-node shell elements are used and 160,514 nodes when 9-node shell elements are used. Although those numbers give insight into how large the computational resources should be, the cost of computation is highly dependent on the computers used by the analyst. To study the effect of the

computational resources on the analysis, the same model is analyzed by two different computers, a workstation and a laptop. Technical details of the computers are listed in Table 3.5., and the solution times are listed in Table 3.6. The laptop is used throughout the study and the workstation is used to compare the computation time. The laptop solved the largest model (h=0.06 and 9-node) in 22 minutes, while the workstation solved the same model in 102 seconds. That clearly shows the importance of the computational resources in the finite element analysis. The amount of time that the laptop took to solve the largest model is too long for the analysis of this problem and that clearly shows the limits of the computational resource of the author. So this element size was chosen to be the smallest one to mesh the model in the mesh density study. However, the following results show that 9-node shell elements converge rapidly and there was no need to use such small elements.

Table 3.5: Technical details of the computers.

	Processor	**RAM**
Laptop	1 X 2.93 GHz Intel Core i7-740QM Processor	4 GB – 1066 MHz DDR3 SD RAM
Workstation	6 X 3.46 GHz Intel Core i7-990X Processor	24 GB – 1333 MHz DDR3 SD RAM

Table 3.6: Solution times for two computers.

	Time [sec]					
	h=0.5		**h=0.1**		**h=0.06**	
	4-node	9-node	4-node	9-node	4-node	9-node
Laptop	0.46	1.84	13.57	75.95	45.16	1,421.44
Workstation	0.31	1.09	7.07	31.29	21.55	102.13

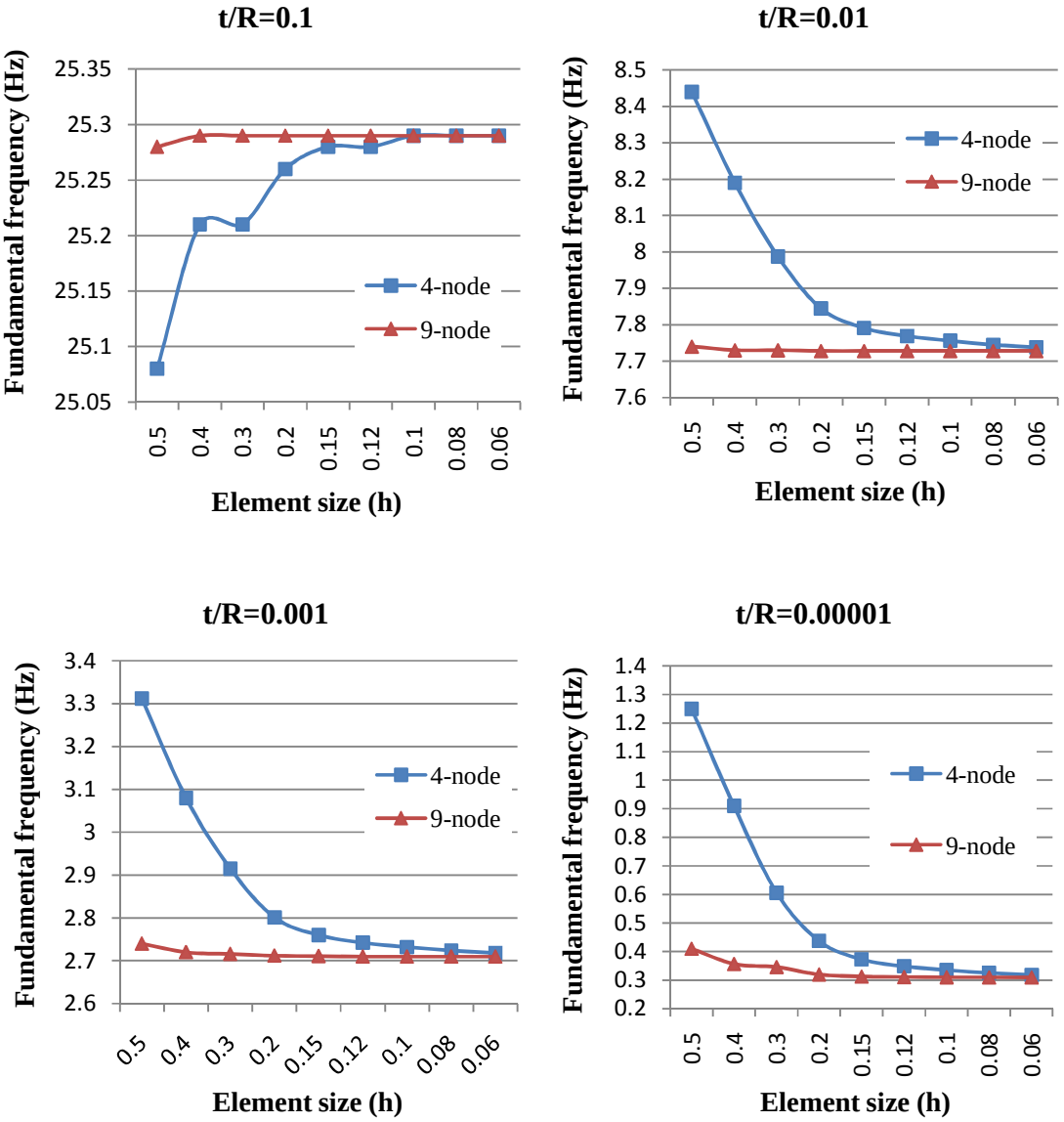

Figure 3.3: Mesh density study.

As presented in Figure 3.3, 9-node shell element converges very quickly while 4-node shell element requires a very fine mesh to reach convergence. For the cylindrical shell with $t/R=10^{-1}$ 4-node shell elements converge when the element sizes are smaller than 0.1. But for the other cylindrical shells, 4-node shell element requires a very fine mesh to converge. In Figure 3.3 it is seen that the 9-node shell element converges to a frequency and keeps getting the same results for the element sizes smaller than 0.1. So considering the computational resources and efficiency issues of the shell elements 9-node shell elements are used to analyze the cylindrical

shells in this thesis. Detailed results of the mesh density study are presented in the following tables.

Table 3.7: The results of the mesh density study for the shell with $t/R=10^{-1}$.

Element Size	Element Type	Fundamental freq. (Hz)	Element Type	Fundamental freq. (Hz)
0.5	4-node shell	25.08	9-node shell	25.28
0.4	4-node shell	25.21	9-node shell	25.29
0.3	4-node shell	25.21	9-node shell	25.29
0.2	4-node shell	25.26	9-node shell	25.29
0.15	4-node shell	25.28	9-node shell	25.29
0.12	4-node shell	25.28	9-node shell	25.29
0.1	4-node shell	25.29	9-node shell	25.29
0.08	4-node shell	25.29	9-node shell	25.29
0.06	4-node shell	25.29	9-node shell	25.29

Table 3.8: The results of the mesh density study for the shell with $t/R=10^{-2}$.

Element Size	Element Type	Fundamental freq. (Hz)	Element Type	Fundamental freq. (Hz)
0.5	4-node shell	8.44	9-node shell	7.74
0.4	4-node shell	8.19	9-node shell	7.73
0.3	4-node shell	7.987	9-node shell	7.73
0.2	4-node shell	7.845	9-node shell	7.728
0.15	4-node shell	7.791	9-node shell	7.728
0.12	4-node shell	7.769	9-node shell	7.728
0.1	4-node shell	7.756	9-node shell	7.728
0.08	4-node shell	7.745	9-node shell	7.728
0.06	4-node shell	7.738	9-node shell	7.728

Table 3.9: The results of the mesh density study for the shell with $t/R=10^{-3}$.

Element Size	Element Type	Fundamental freq. (Hz)	Element Type	Fundamental freq. (Hz)
0.5	4-node shell	3.312	9-node shell	2.74
0.4	4-node shell	3.08	9-node shell	2.72
0.3	4-node shell	2.915	9-node shell	2.716
0.2	4-node shell	2.801	9-node shell	2.712
0.15	4-node shell	2.76	9-node shell	2.711
0.12	4-node shell	2.742	9-node shell	2.71
0.1	4-node shell	2.732	9-node shell	2.71
0.08	4-node shell	2.724	9-node shell	2.71
0.06	4-node shell	2.718	9-node shell	2.71

Table 3.10: The results of the mesh density study for the shell with $t/R=10^{-5}$.

Element Size	Element Type	Fundamental freq. (Hz)	Element Type	Fundamental freq. (Hz)
0.5	4-node shell	1.25	9-node shell	0.41
0.4	4-node shell	0.91	9-node shell	0.3566
0.3	4-node shell	0.6061	9-node shell	0.3456
0.2	4-node shell	0.4372	9-node shell	0.3195
0.15	4-node shell	0.373	9-node shell	0.3123
0.12	4-node shell	0.3486	9-node shell	0.3105
0.1	4-node shell	0.3353	9-node shell	0.3098
0.08	4-node shell	0.3254	9-node shell	0.3098
0.06	4-node shell	0.3182	9-node shell	0.3098

4. Free Vibrations of the Unstiffened Cylindrical Shell

4.1 An Introduction on the Study of the Unstiffened Cylindrical Shell

In this section of the thesis, the unstiffened cylindrical shell is analyzed. This study consists of two parts: Free vibrations of the unstiffened cylindrical shells without initial stress conditions and free vibrations of unstiffened cylindrical shells with initial stress conditions. Free vibration characteristics of unstiffened cylindrical shells, the correlation between the thickness change and the frequency variation, and the effect of initial stress on the free vibration modes of unstiffened cylindrical shells are studied.

The study is carried out by analyzing four unstiffened cylindrical shells, each having different thicknesses. Their thickness parameters are $t/R=10^{-1}$, $t/R=10^{-2}$, $t/R=10^{-3}$ and $t/R=10^{-5}$. The cylindrical shell with $t/R=10^{-2}$ is a very similar model to a real submarine considering the dimensions. In the first part of this section, the models are analyzed without applying initial stresses to them. The vibration modes and the variation of the frequencies with the thickness change are studied. In the second part, initial compressive and tensile membrane stresses are applied separately on the cylindrical shells and the effect of the initial stresses on the free vibration modes is studied.

4.2 Results of the Finite Element Solution for the Unstiffened Cylindrical Shells

The unstiffened cylindrical shells are analyzed. The characteristics of free vibrations of unstiffened cylindrical shells, variation of the frequencies with the thickness change and the effect of initial membrane stresses on the unstiffened cylindrical shells are studied. The results show that changing the thickness significantly influences the free vibration modes of the cylindrical shells. The frequencies of the cylindrical shell increase as the shell gets thicker. The change of the frequencies with the change of the thickness gives important information about bending and membrane behavior of the cylindrical shells.

Initially applied membrane stresses affect the vibration modes of the cylindrical shell significantly. Tensile stresses increase the frequencies of the cylindrical shells while the compressive stresses decrease the frequencies. It is known that there is a correlation between the

frequency behavior and the buckling behavior of cylindrical shells [1]. This study showed that initially applied compressive stresses reduce the stiffness of the cylindrical shell and their frequencies approach zero. An important result of this study is that initially applied membrane stresses restrict the rigid body rotations of the unstiffened cylindrical shells. The unstiffened unstressed cylindrical shell has six rigid body modes and six zero frequencies corresponding to those rigid body modes. But when initial tensile stresses are applied on the cylindrical shell, although it still has six rigid body modes, its three rigid body rotations are restricted and their frequencies are very small but not zero. Detailed information on the study is presented in the following sections.

4.2.1 Free vibration characteristics of the unstiffened cylindrical shells

Four cylindrical shells, each of them having different thicknesses, are analyzed to study the free vibration modes of unstiffened cylindrical shells. First twenty six modes (including rigid body modes) of the shells are calculated. The aim of the study is to see how the free vibration modes are affected with the change in the thickness of the shell.

Results show that the cylindrical shell has multiple frequencies because of the symmetry. In Figure 4.1 the frequencies of the four cylindrical shells are presented. The multiple frequencies can be observed in Figure 4.1.

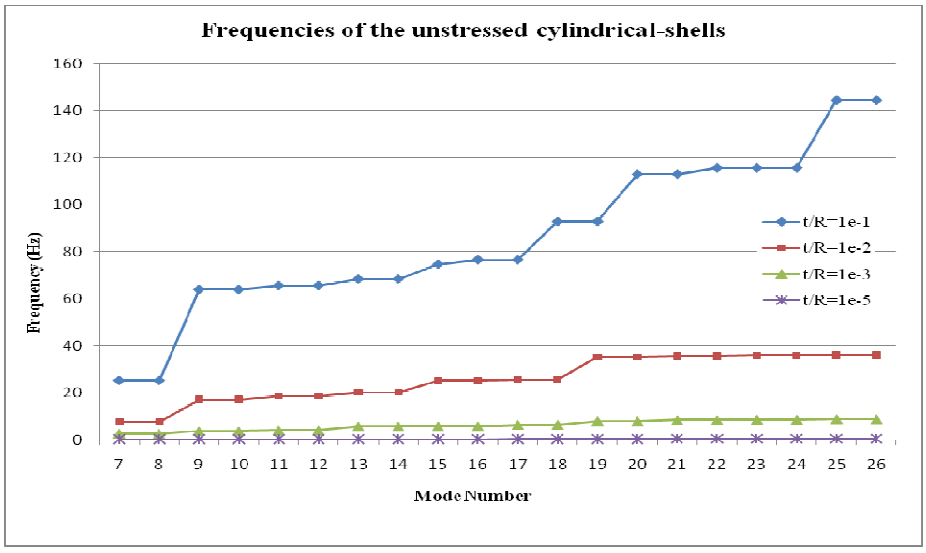

Figure 4.1: The frequencies of the unstressed cylindrical shells.

Two consecutive modes have the same frequencies. The only exception is that, Mode 15 of the cylindrical shell with $t/R=10^{-1}$ has a unique frequency. This mode corresponds to a torsional mode and it doesn't have a multiple frequency as it is seen in the other modes. In the other modes, two consecutive frequencies are equal and the mode shapes are rigid body rotations. This rotation can be seen in Figure 4.2.

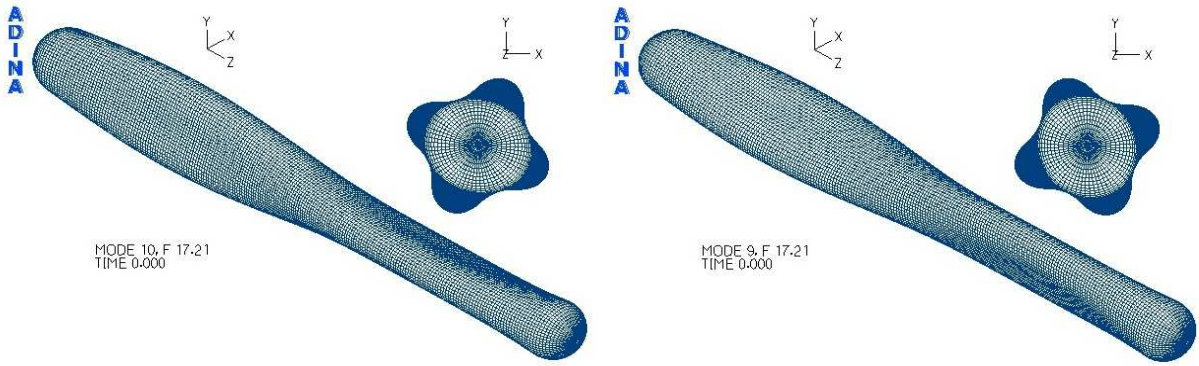

Figure 4.2: Rigid body rotation between two consecutive modes.

The mode shapes of the cylindrical shells are highly dependent on the thickness. Detailed information regarding the wave numbers and frequencies can be found in Table 4.1. For the thickest cylindrical shell ($t/R=10^{-1}$), the number of circumferential full waves (n) remains constant and the number of longitudinal half waves (m) increases consecutively with the mode number. Contrary to the mode shape pattern of the thickest cylindrical shell, the other three cylindrical shells have fewer longitudinal half waves than the circumferential full waves. The number of circumferential waves changes with the mode number while the number of longitudinal waves usually remains constant and small compared to the circumferential waves. Only exception is in the modes 23 and 24 of the cylindrical shell with $t/R=10^{-2}$. In those modes, the number of longitudinal waves is bigger than the number of circumferential waves. Those modes are an exception and thinner cylindrical shells have more circumferential waves than longitudinal waves. As the shell gets thinner it makes more circumferential waves and fewer longitudinal waves.

Table 4.1: Frequencies of the cylindrical shell with different thicknesses.

Mode Number	t/R=1e-1			t/R=1e-2			t/R=1e-3			t/R=1e-5		
	Freq.(Hz)	n	m	Freq.(Hz)	n	m	Freq.(Hz)	n	m	Freq.(Hz)	n	m
7	25.29	Bending Mode		7.728	2	1	2.71	3	1	0.3098	9	1
8	25.29	Bending Mode		7.728	2	1	2.71	3	1	0.3098	9	1
9	63.98	Bending Mode		17.21	2	2	3.742	4	1	0.3109	10	1
10	63.98	Bending Mode		17.21	2	2	3.742	4	1	0.3109	10	1
11	65.7	2	1	18.69	3	1	4.093	2	1	0.3351	11	1
12	65.7	2	1	18.69	3	1	4.093	2	1	0.3351	11	1
13	68.48	2	2	20.29	3	2	5.804	5	1	0.3398	8	1
14	68.48	2	2	20.29	3	2	5.804	5	1	0.3398	8	1
15	74.75	Torsional Mode		25.27	Bending Mode		5.825	4	2	0.3756	12	1
16	76.75	2	3	25.27	Bending Mode		5.825	4	2	0.3756	12	1
17	76.75	2	3	25.74	3	3	6.509	5	2	0.4106	7	1
18	92.96	2	4	25.74	3	3	6.509	5	2	0.4106	7	1
19	92.96	2	4	35.3	2	3	8.049	3	2	0.4279	13	1
20	113.1	Bending Mode		35.3	2	3	8.049	3	2	0.4279	13	1
21	113.1	Bending Mode		35.72	4	1	8.457	6	1	0.4894	14	1
22	115.8	2	5	35.72	4	1	8.457	6	1	0.4894	14	1
23	115.8	2	5	35.98	3	4	8.719	6	2	0.5379	6	1
24	115.8	0	0	35.98	3	4	8.719	6	2	0.5379	6	1
25	144.6	2	6	36.14	4	2	8.892	5	3	0.5584	15	1
26	144.6	2	6	36.14	4	2	8.892	5	3	0.5584	15	1

n: number of circumferential waves.
m: number of longitudinal half waves.

The variation of the frequencies with the mode number is not the same for all cylindrical shells considered in this study. As the shell thickness increases, the discrepancy between consecutive frequencies gets bigger. In Figure 4.1 it is seen that the slope of the line for the thickest shell is the highest. As the shell gets thinner the slope decreases. That can be explained by studying the effect of the thickness in the analytical expression for the frequencies of the cylindrical shells. The analytical expression is presented in Section 4.3.1. In the analytical expression for the frequency (4.1), the thickness is a multiplier of the wave numbers. Changing the mode means changing the wave numbers in the solution. Since we have the same material properties and the geometry except the thickness, only variables are the wave numbers and the thickness in the formula. Considering that the thickness is the multiplier of the wave number, it is concluded that there is a relation between the thickness and the discrepancy between the

frequencies of two consecutive modes. So as the shell gets thicker, the differences between the frequencies of the same cylindrical shell increases.

In bending and torsional modes, the cylindrical shells are bent or twisted as a whole structure. That is, they don't make any waves in both directions and they deform globally. Results show that the bending and torsional modes occur at higher frequencies. The cylindrical shells with $t/R=10^{-1}$ and $t/R=10^{-2}$ have bending modes and only the cylindrical shell with $t/R=10^{-1}$ has a torsional mode. The thinner cylindrical shells have neither bending nor torsional modes since their lowest twenty six frequencies are not high enough. Some examples of bending and torsional modes seen in this study are presented in Figure 4.3.

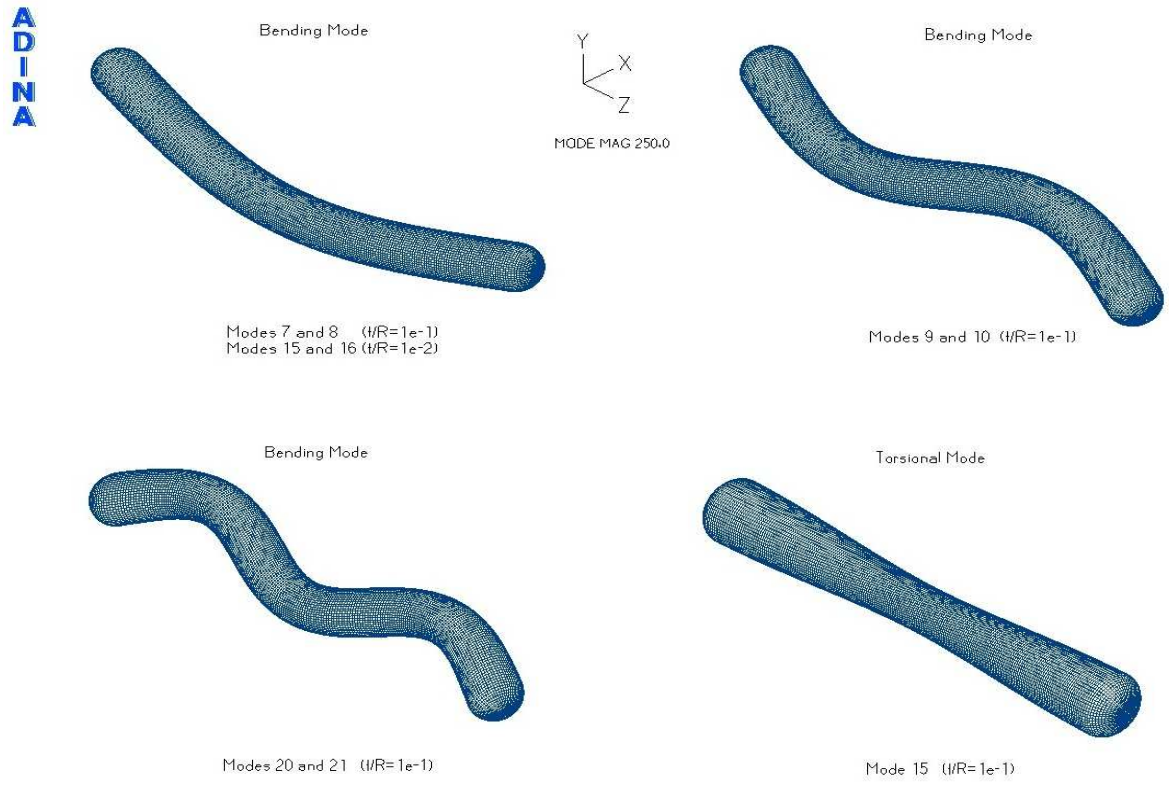

Figure 4.3: Bending and torsional modes for the cylindrical shells.

The correlation between the thickness change and the frequency variation is an interesting subject to study on. Artioli *et al.* [15] focus on the asymptotic behavior of the lowest frequency, as the thickness approaches zero. The authors consider the free vibration problem of thin shells of revolution of constant type of geometry. They compared the theoretical results with

two different numerical discretization procedures they carried out in the study. It is concluded that the numerical results are in agreement with the theoretical results. An important outcome of this study which is related to this thesis is that for parabolic fully clamped shell of revolution, the first eigenfrequency behaves like square root of the thickness. That means that the frequency can be scaled with square root of the thickness. The term “parabolic” shell defines a shell which has zero Gaussian curvature (e.g. cylindrical shells, conical shells)[3]. The cylindrical shell studied in this thesis is a parabolic shell.

Chapelle and Bathe [3] have considered a cylindrical shell with both ends clamped as an example for the asymptotic considerations in dynamic analysis. The authors have solved the problem for four different shell thicknesses using ADINA. The study presented in [3] is similar to the study carried out in this thesis for the unstiffened cylindrical shells. Ref. [3] is an important reference to verify the observations made in this thesis.

In order to study the correlation between the thickness change and the frequency variation, first the similarity between the cylindrical shell considered here and the models considered in [3,15] should be reviewed. The cylindrical part of our model (excluding the hemispheres) is a parabolic shell. The cylindrical shell has hemispherical end closures at both ends. It is expected that the end closures restrict the displacements in the radial direction at both ends. As a result of this constraint at the ends, the cylindrical shell can be thought as a cylindrical shell with simply supported or clamped boundary conditions at the ends. It is not very important to strictly determine if the assumption should be made for simply supported or clamped boundary conditions because the effect of the boundary conditions decreases as L/R for the cylindrical shell increases [1]. So our model can be related to the models considered in [3,15].

The unstiffened cylindrical shells studied in this thesis can be considered as membrane dominated and it is expected that their lower frequencies scale as $\sqrt{t}$. Results of the analyses carried out here show that the frequencies are changing approximately by the order of square root of the thickness change. The variation of the fundamental frequencies of the cylindrical shells with $t/R=10^{-3}$ and $t/R=10^{-5}$ will be studied as an example. The cylindrical shell with $t/R=10^{-3}$ is 100 times thicker than the cylindrical shell with $t/R=10^{-5}$. The fundamental frequency of the cylindrical shell with $t/R=10^{-3}$ (2.71 Hz) is approximately 10 times of the fundamental

frequency of the cylindrical shell with t/R=10^{-5} (0.31 Hz). So the ratio between the fundamental frequencies is approximately 10, which is equal to the square root of the ratio between the thicknesses. Detailed results are listed in the Table 4.1. The results show that the discussion for the change of the frequencies with the change of the thickness is valid for the cylindrical shells studied in this thesis. Especially in the lower modes scaling of the frequencies with √t is more closely present. It is concluded that the unstiffened cylindrical shells studied in this thesis is mostly membrane dominated and good results are obtained in this section. The results obtained in this study are also consistent with the discussions made in Ref. [3,15].

4.3 Comparison of the Finite Element Solution with the Analytical Solution

In this chapter, the free vibration problem of the unstiffened cylindrical shell is first solved using finite element procedures in ADINA. To be able to verify the results of the finite element solution and to address the differences between the analytical and finite element solution for this problem, in the next sections two solutions will be compared.

4.3.1 The analytical solution for the free vibration problem of the unstiffened cylindrical shells

The analytical solution of the free vibration problem of the cylindrical shell is presented in [16]. The authors start with the differential equations of motion for a freely vibrating cylindrical shell in the framework of Donnell-Mushtari-Vlasov theory. They assume that the cylinder is simply supported and postulate a form of the solution which is satisfying the boundary conditions. Using the displacement components of the postulated solution in the differential equations of motion for the cylindrical shell leads to an eigenvalue problem. The solution of this eigenvalue problem gives the natural frequencies and the numbers of circumferential and longitudinal waves. So the solution gives the natural frequency and the corresponding mode shape. Details and the step by step solution of the problem is presented in [16]. The equation for the natural frequencies of the unstiffened cylindrical shell is

$$\omega^2 = \frac{E}{\rho R^2(1-\nu^2)} \frac{(1-\nu^2)\lambda^4 + a^2(\lambda^2+n^2)^4}{n^2+(\lambda^2+n^2)^2} \tag{4.1}$$

where n is the number circumferential half waves, m is the number of longitudinal full waves, $\lambda = \frac{m\,\pi R}{L}$ and $a^2 = \frac{t^2}{12\,R^2}$.

4.3.2 Comparing the finite element solution with the analytical solution

In this chapter of the thesis free vibration problems of four unstiffened cylindrical shells are solved in ADINA. To compare the results of the finite element solution with the analytical solution, two of them are analyzed analytically, using (4.1). The considered cylindrical shells are the shells with $t/R=10^{-2}$ and $t/R=10^{-3}$. The frequencies of the vibration modes in which the cylindrical shell is making one longitudinal half wave are calculated for increasing number of circumferential full waves. The change of those particular frequencies with the number of circumferential full waves is plotted to compare the results. The plots for both models are shown in Figure 4.4.

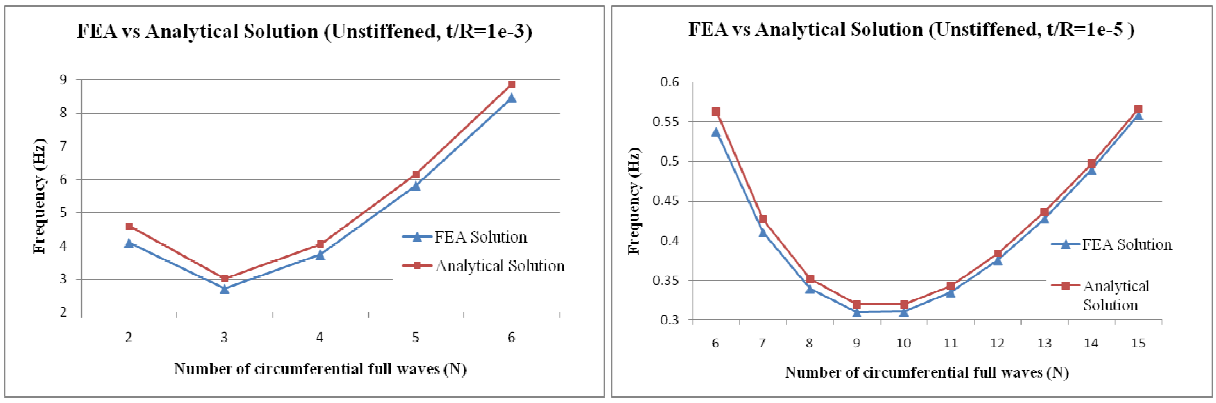

Figure 4.4: Variation of the frequencies with the number of circumferential waves (m=1).

Figure 4.4 shows that the variations of the frequencies with the number of circumferential waves for both solutions. The results are qualitatively and quantitatively very similar. There are slight differences in the frequencies but it can be concluded that good results are obtained for the finite element solution. The discrepancy of the frequencies results from the difference in the assumptions made in both solutions. The finite element solution calculates lower frequencies for both cylindrical shells than the analytical solution. That result implies that the analytical model is stiffer than the finite element model. Since the geometry and the material properties of both models are the same, the boundary conditions should be studied to explain why the frequencies

are slightly different. In Section 4.3.1 it is noted that the postulated solution satisfies the simply supported boundary conditions. That is, the cylindrical shell is simply supported at both ends. The simply supported boundary condition restricts the axial and lateral deflections at the ends. In the finite element model the cylindrical shell is closed with hemispheres at both ends. The cylindrical shell is free to move in the axial direction but the lateral deflections are somewhat restricted with the end closures. So the movements of the finite element model at the ends are not restricted as rigidly as in the model of the analytical solution. As a result, the frequencies of the finite element solution are lower than those of the analytical solution. Although there are discrepancies in the frequencies, it can be concluded that the assumption for the boundary conditions in the analytical solution is successful for the model considered in this thesis. Comparison of the results verifies that good results are obtained in the finite element analysis.

4.4 Free Vibrations of the Pre-stressed Cylindrical Shell

In the preceding sections free vibrations of unstiffened cylindrical shell with different thicknesses are studied. Throughout this study linear analysis conditions are considered. In large deformation analysis membrane stresses can be present and those stresses highly affect the dynamic behavior. In this section, the effect of the initial membrane stresses on the free vibration characteristic of the unstiffened cylindrical shell is studied. The shell geometry, the boundary conditions and the material properties are all the same as before. The only difference is that the cylindrical shells are pre-stressed. An initial hoop stress of $2.44\text{x}10^7$ Pa and an initial longitudinal stress of $1.22\text{x}10^7$ Pa are applied to all four cylindrical shells with different thicknesses. In order to satisfy stress continuity between the cylindrical part and the hemispherical part of the model an initial stress of $1.22\text{x}10^7$ Pa is applied to the hemispherical shells which are located at both ends. The stresses are applied in both compressive and tensile states in separate analyses. These initial tensile stresses resemble the stress state in a pressure vessel with an internal applied pressure of $p = 2.44 \times 10^7 (t/R)$ while the initial compressive stresses resemble the stress state in a submarine with an external applied pressure of the same value.

The tensile stress is applied to four cylindrical shells with different thicknesses and the first 16 frequencies and mode shapes (including rigid body modes) are calculated in ADINA.

The variation of the frequencies with the mode numbers is presented in Figure 4.5 and the results are listed in Table 4.2. It is obvious that the initial tensile stress is increasing the frequencies of the cylindrical shell. The amount of the increase is very small for the thickest shell while the frequencies of the thinner shells increase significantly. The frequencies in the lower modes increase more compared to those in the higher modes of the same model. The effect of the initial tensile stress can be observed better in the lower modes. The following observations are made for the tensile pre-stressed cylindrical shell:

- For the thickest cylindrical shell ($t/R=10^{-1}$), there is a slight increase in the frequencies. The maximum increase is less than 2%. The mode shapes are exactly the same as the mode shapes of the unstressed cylindrical shell.

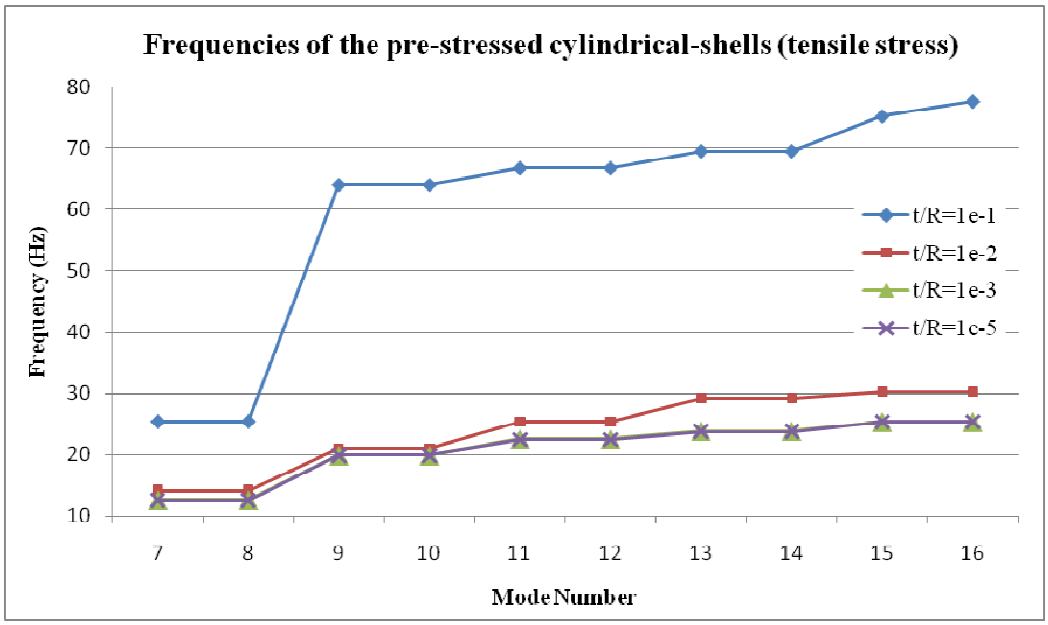

Figure 4.5: Frequencies of the pre-stressed cylindrical shells (tensile stress).

Table 4.2: Frequencies of the pre-stressed cylindrical shell with different thicknesses (tensile stress).

Mode Number	t/R=1e-1			t/R=1e-2			t/R=1e-3			t/R=1e-5		
	Freq.(Hz)	n	m	Freq.(Hz)	n	m	Freq.(Hz)	n	m	Freq.(Hz)	n	m
1	Rigid body motions.			Rigid body motions.			Rigid body motions.			Rigid body motions.		
2												
3												
4	1.366	R. B. Rotations		1.366	R. B. Rotations		1.366	R. B. Rotations		1.366	R. B. Rotations	
5	1.366			1.366			1.366			1.366		
6	8.856			8.867			8.867			8.867		
7	25.43	Bending Mode		14.22	2	1	12.61	2	1	12.6	2	1
8	25.43	Bending Mode		14.22	2	1	12.61	2	1	12.6	2	1
9	64.08	Bending Mode		21	2	2	19.91	2	2	19.9	2	2
10	64.08	Bending Mode		21	2	2	19.91	2	2	19.9	2	2
11	66.82	2	1	25.4	Bending Mode		22.62	3	1	22.54	3	1
12	66.82	2	1	25.4	Bending Mode		22.62	3	1	22.54	3	1
13	69.57	2	2	29.23	3	1	23.91	3	2	23.83	3	2
14	69.57	2	2	29.23	3	1	23.91	3	2	23.83	3	2
15	75.28	Torsional Mode		30.32	3	2	25.4	Bending Mode		25.4	Bending Mode	
16	77.72	2	3	30.32	3	2	25.4	Bending Mode		25.4	Bending Mode	

n: number of circumferential waves.
m: number of longitudinal half waves.

- For the cylindrical shell with $t/R=10^{-2}$, the frequencies increase considerably compared to those of the unstressed cylindrical shell. The lowest two frequencies increase by 84% while the others increase approximately by 30-40%. The effect of the initial tensile stress is much higher for the lowest frequencies. Although the frequencies change significantly, the mode shapes are very similar to those of the unstressed cylindrical shell. But for the pre-stressed cylindrical shell the bending mode occurs in modes 11 and 12 instead of modes 15 and 16 as for the unstressed shell.

- For the cylindrical shell with $t/R=10^{-3}$, the increase in the frequencies are significant. The frequencies increase by 350-400% and the mode shapes change drastically. The mode shape pattern becomes very similar to that of the thicker cylindrical shells. The number of the circumferential waves decreases. After initial tensile stress is applied on the thin cylindrical shell, it makes fewer circumferential waves like the thick cylindrical shell. Unlike the unstressed cylindrical shell of the same geometry, a bending mode occurs in modes 15 and 16 when initial tensile stress is applied.

- For the cylindrical shell with $t/R=10^{-5}$, the results are very similar to those of the pre-stressed cylindrical shell with $t/R=10^{-3}$ in terms of the frequencies and mode shapes. These two

thin shells become very stiff under tensile pre-stress conditions compared to the unstressed cylindrical shells of the same thicknesses. As a result of this stiffening effect they start to act like thicker shells. That is, their mode shape patterns become very similar to the mode shape patterns of the thicker shells.

- The asymptotic behavior of the pre-stressed cylindrical shell (as its thickness is reduced) is different than that of the unstressed cylindrical shell. Because of the stiffening effect resulting from initial membrane stresses, the lowest frequencies of the pre-stressed cylindrical shell converge to a thickness invariant value for the lowest frequency. In our particular solution the lowest frequencies of the two thinnest shells converged to the value of 12.60 Hz. However in Section 4.2.1 it is discussed that, for the unstressed cylindrical shell the lowest frequency scaled approximately as $\sqrt{t}$. Figure 4.5 shows that the higher frequencies of the cylindrical shells with $t/R=10^{-3}$ and $t/R=10^{-5}$ are also very similar.

- An interesting observation is that the initially applied membrane stresses restrict the rigid body rotations of the cylindrical shells. The unstressed cylindrical shell has six rigid body modes and the lowest six frequencies are zero as expected since the model is free in space. The 4^{th}, 5^{th} and 6^{th} frequencies of the pre-stressed cylindrical shell are nonzero unlike those of the unstressed cylindrical shell, although the pre-stressed shell still has the rigid body modes. Those nonzero frequencies are very small and correspond to rigid body rotations. This is an effect of the initial tensile membrane stress. It is noticed that the frequencies are very small and this is due to the initial loading not being deformation dependent. In the formulation of the stiffness matrix, the effect of the initial stresses enters the nonlinear stiffness matrix and the nonlinear stiffness matrix is independent of rotation. As a result, the initial membrane stresses restrict the rigid body rotations and we see very small frequencies in the corresponding modes. A detailed explanation of this formulation is presented in [5]. An example problem on the free vibrations of a truss element is demonstrated in Appendix A in order to explain the effect of the initial stress on the rigid body modes.

In summary, initially applied tensile membrane stresses make the cylindrical shell stiffer compared to the unstressed cylindrical shell. The frequencies of the pre-stressed cylindrical shell are higher than those of the unstressed cylindrical shell and the mode shapes of the two thinnest shells change significantly.

The initial compressive stress is also applied on the cylindrical shells with four different thicknesses. The geometry, the material conditions and the amount of the stress is all as before. Only difference is that the initially applied membrane stresses are compressive in this part of the study. Considering the results of the tensile pre-stressed cylindrical shell, it is expected that the frequencies decrease when the initial compressive stress is applied on the shell.

The initial compressive stress is applied to four of the cylindrical shells. For the two thinnest shells ($t/R=10^{-3}$, $t/R=10^{-5}$), the solution process is stopped in ADINA since the frequencies approach zero. So the first 16 frequencies and mode shapes (including rigid body modes) of the two thickest cylindrical shells ($t/R=10^{-1}$, $t/R=10^{-2}$) are calculated. The results are listed in Table 4.3 and the following observations are made:

- For the cylindrical shell with $t/R=10^{-1}$, there is a slight decrease in the frequencies. The maximum decrease is less than 2%. The mode shapes are exactly the same as the mode shapes of the unstressed cylindrical shell.
- For the cylindrical shell with $t/R=10^{-2}$, the frequencies decreased significantly compared to the unstressed cylindrical shell. The lowest twelve frequencies approach zero. First six modes are not rigid body motions but their frequencies are nearly zero and the shell is affected significantly by the initial compressive stress. From 6^{th} to 12^{th} modes are rigid body modes and the corresponding frequencies are approximately zero. The shell is significantly affected by the initial compressive stress and its frequencies decrease drastically.

In this study, the initial compressive membrane stress resembles the stress state in a submarine with an external applied pressure of $p = 2.44 \times 10^7 (t/R)$. Norwood [1] discussed the influence of the ring stiffeners, boundary conditions, end closures, external pressure loading and added mass of the surrounding fluid on the vibrational modes of the cylindrical shell with a review of the available literature. The author has noted that an increase in the external hydrostatic pressure acting on the cylindrical shell decreases the frequencies [1]. As the external hydrostatic pressure approaches the buckling pressure of the cylindrical shell, the frequencies approach zero. This is an important correlation between the frequency behavior and the buckling behavior of the cylindrical shell. The purpose of this section of the thesis is to study the effect of initial stress on the frequencies of cylindrical shell. So only a constant compressive stress is

applied to the cylindrical shells. For further study the variation of the frequencies of the same cylindrical shell with the variation of the compressive stresses could be studied.

Table 4.3: Frequencies of the compressive pre-stressed cylindrical shell with different thicknesses**.**

Mode Number	t/R=1e-1			t/R=1e-2		
	Freq.(Hz)	n	m	Freq.(Hz)	n	m
1	1.59E-06	Rigid body motions.		1.59E-06	3	1
2	1.59E-06	Rigid body motions.		1.59E-06	3	1
3	1.59E-06	Rigid body motions.		1.59E-06	3	2
4	1.74E-04	Rigid body motions.		1.59E-06	3	2
5	1.97E-04	Rigid body motions.		1.59E-06	2	1
6	3.01E-04	Rigid body motions.		1.59E-06	2	1
7	25.16	Bending Mode		1.59E-06	Rigid body motions.	
8	25.16	Bending Mode		1.59E-06	Rigid body motions.	
9	63.87	Bending Mode		1.59E-06	Rigid body motions.	
10	63.87	Bending Mode		1.59E-06	Rigid body motions.	
11	64.66	2	1	1.59E-06	Rigid body motions.	
12	64.66	2	1	1.59E-06	Rigid body motions.	
13	67.46	2	2	12.31	2	2
14	67.46	2	2	12.31	2	2
15	74.22	Torsional Mode		12.34	3	3
16	74.78	2	3	12.34	3	3

n: number of circumferential waves.
m: number of longitudinal half waves.

5. Free Vibrations of the Stiffened Cylindrical Shell

5.1 An Introduction on the Study of the Stiffened Cylindrical Shell

In this section of study, frequencies and mode shapes of stiffened cylindrical shells are analyzed. This study consists of two parts: variation of the frequencies with the positions of the ring stiffeners and variation of the frequencies with the number of uniformly distributed ring stiffeners. Two of the cylindrical shells used in previous section of the research are used. These are the "thick" cylindrical shell with $t/R=10^{-2}$ and the "thin" cylindrical shell with $t/R=10^{-3.}$ Ring stiffeners are used to stiffen the shells.

Free vibrations of stiffened and unstiffened cylindrical shells are studied by many researchers. Among those [1,4] are used as references in the process of this study. In [4] a study on the vibration of thin cylindrical shells with ring supports is presented. In the study, Sanders' shell theory is used and the governing equations for vibrations are obtained using an energy functional with the Ritz method. The authors have validated the analysis by comparing the results with those available in the literature. Loy and Lam [4] focus on the influence of the position of the ring stiffener and boundary conditions on ring-stiffened cylindrical shells with different thicknesses and lengths. In [4] it is concluded that a ring stiffener has significant influence on the frequencies, and the extent of this influence depends on the position of the ring stiffener and the boundary conditions of the cylindrical shell.

In [1] the modal behavior of the ring-stiffened cylindrical shells is reviewed. In the study, the effect of the ring stiffeners, boundary conditions, end closures, external pressure loading and added mass of the surrounding fluid are discussed. The author reviews the available literature and discusses the influence of those factors on the vibrational modes of the cylindrical shell. In [1] it is concluded that the free vibrational modes of the cylindrical shells are affected by ring stiffeners, boundary conditions, end closures, external pressure loading and added mass of the surrounding fluid. The external pressure and surrounding mass of water reduces the frequencies while the ring stiffeners increase the frequencies when compared to unstiffened cylindrical shells. The effect of boundary conditions and end closures are related to the types of conditions used in the model.

In this study, first uniformly distributed ring stiffeners are added to the cylindrical shells. According to the results, when the shell displaces into circumferential waves, the frequencies increase with the number of stiffeners. But frequencies of the cylindrical shell with one stiffener at the center are higher than those of the cylindrical shell with two stiffeners at both ends of the cylinder. This result shows that the positions of the ring stiffeners are as important as their number. Then, to study the variation of the frequencies with the position of the ring stiffeners, just two stiffeners are added to the shells and the positions of the ring stiffeners are changed at every step. The study on the variation of the frequencies with the position of the ring stiffeners gives insight to understand and interpret the results of the uniformly-stiffened cylindrical shells.

5.2 The Finite Element Model of the Ring-Stiffened Cylindrical Shell

The dimensions used for the "thick" cylindrical shell ($t/R=10^{-2}$) are very similar to those of a real submarine. When modeling ring stiffeners, the dimensions are adopted from the ring stiffeners used in the construction of the same type of submarines from which the dimensions are adopted to model the "thick" cylindrical shell. The stiffeners of the real model have T cross-sections. To model curved beams in ADINA, a rectangular cross section which has the same moment of inertia (I) as the T cross-section is defined and used. The calculation of the equivalent dimensions for the rectangular cross section is presented in Appendix B.

In the finite element model, the surface of the cylinder is meshed with the 9-node shell elements. A detailed study on choosing the proper element type and mesh density is presented in Section 3.3. To model the stiffened cylindrical shell, ring stiffeners are added to the model and they are modeled as curved beams and meshed with the 3-node iso-beam elements. Figure 5.1 shows a stiffened cylindrical shell. The ring stiffeners are attached to the inside surface of the cylinder. To be able to show the ring stiffeners in the figure, the cylindrical shell is cut through a plane which is positioned at x=0.

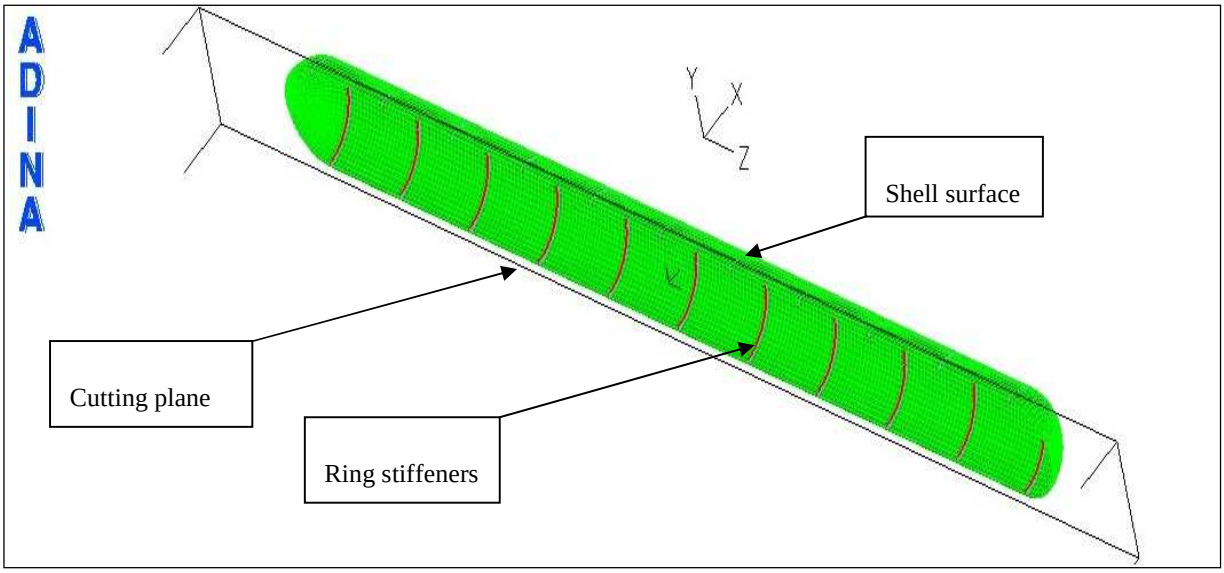

Figure 5.1: The stiffened cylindrical shell.

Iso-beam elements are attached to shell elements using rigid links to model the stiffened cylindrical shell. Figure 5.2 presents a cross-section of a single shell and beam connection. The schematic shows where the nodes are positioned and how the rigid link is used to connect shell and beam elements. Detailed picture of the ring stiffeners and the rigid links in the finite element model is presented in Figure 5.3.

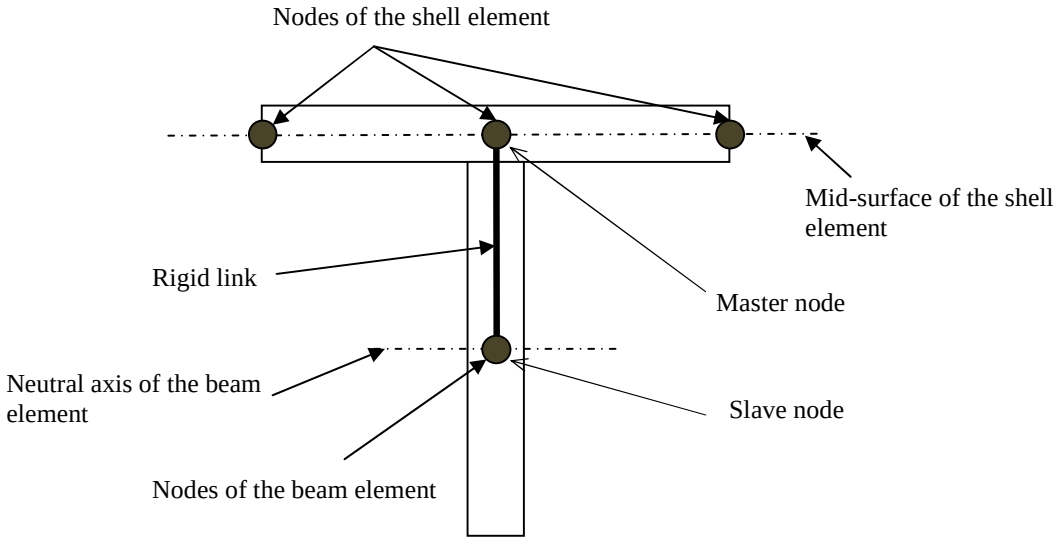

Figure 5.2: The schematic of the connection between shell and beam elements.

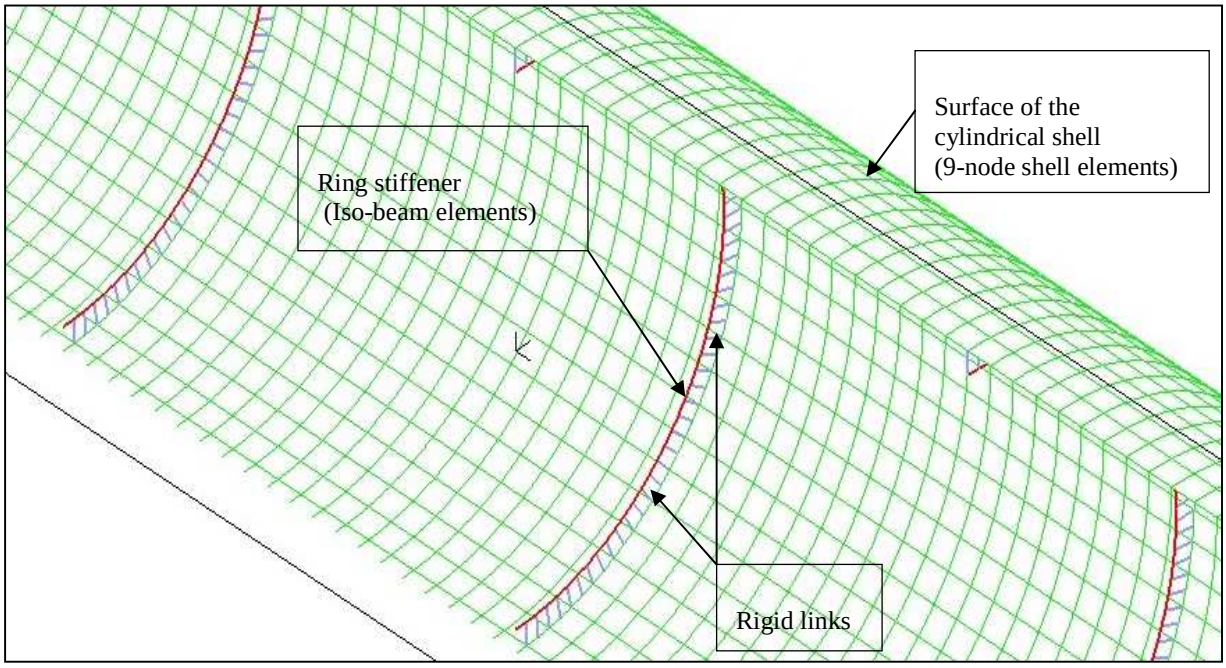

Figure 5.3: A detailed representation of the ring stiffeners and the rigid links.

5.3 Results of the Finite Element Solution for the Stiffened Cylindrical Shells

The ring-stiffened cylindrical shells are analyzed. Results show that frequencies increase with the number of stiffeners when the cylindrical shell makes circumferential waves. If the cylindrical shell does not undergo any circumferential waves, which corresponds to its bending modes, the frequencies of the cylindrical shells with different thicknesses are very close and decrease slightly when more ring stiffeners are added.

An interesting result is that the positions of the ring stiffeners are as important as their number when contributing to the stiffness of whole structure. All detailed results are presented in the tables in Appendix C.

5.3.1 Variation of the Fundamental Frequencies with the Positions of the Ring Stiffeners

In general, adding ring stiffeners to the cylindrical shell increases the stiffness and increases the frequencies of the cylindrical shell. So the cylindrical shell with more ring stiffeners has higher frequencies than the one with fewer ring stiffeners. An exception is that one

stiffener positioned at the center of the cylinder is contributing more to the stiffness than two stiffeners positioned at both ends of the cylinder. Detailed results are presented in Figure 5.4 and listed in the tables in Appendix C.

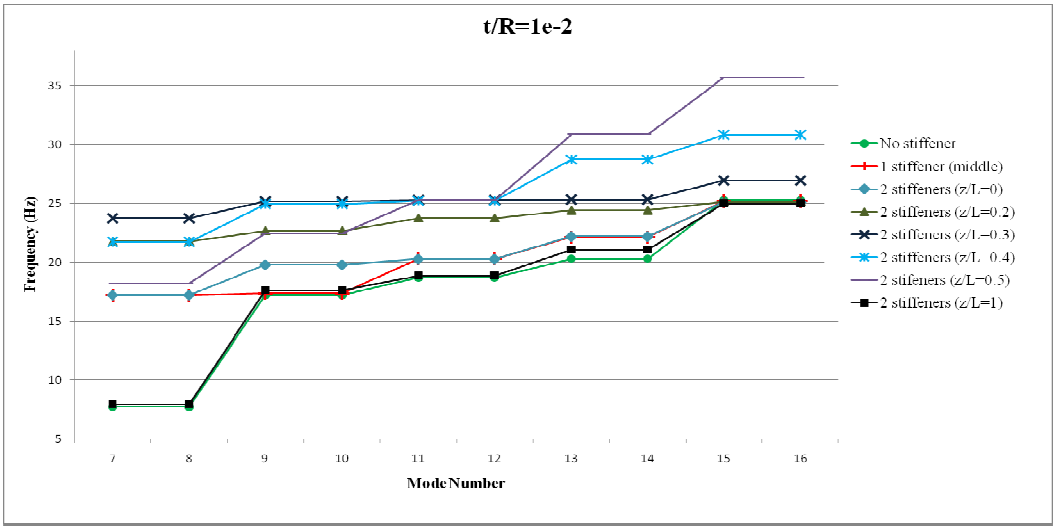

Figure 5.4: The frequencies of thick cylindrical shell ($t/R=10^{-2}$) at different positions of the ring stiffeners.

The positions of the ring stiffeners have a big role in the contribution of the stiffeners to stiffness. In [4] it is shown that the frequency of the cylindrical shell varies with the position of the ring stiffener. In order to study this phenomenon, two stiffeners are positioned at different distances from the center of the cylinder in the longitudinal direction and the results are compared. When presenting the results, distance from the center of the cylinder in the longitudinal direction is scaled with the half length of the cylinder and absolute value of this ratio is taken to be able to represent both directions. The distances and the reference coordinate system are presented in Figure 5.5.

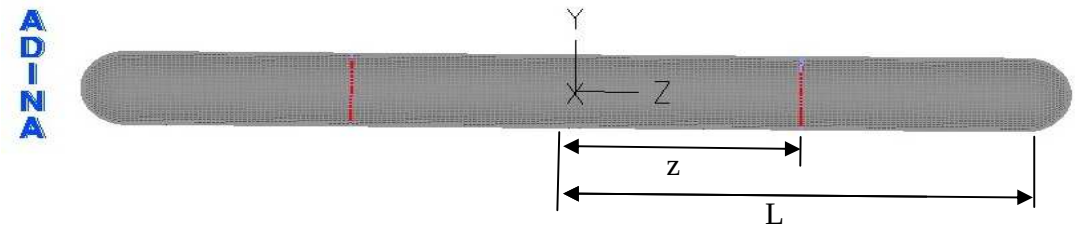

Figure 5.5: Positions of the ring stiffeners.

For both cylindrical shells, it is seen that the frequencies increase as the stiffeners get closer to the center of the cylinder (z=0) up to a critical distance. At the critical distance frequencies reach their maximum values. After the critical distance they start to decrease and they converge to the frequency of the cylindrical shell with one stiffener positioned at the center.

For the thick cylindrical shell, two stiffeners positioned at both ends make a very little contribution to the frequency increase. Figure 5.4 shows that the frequencies of the unstiffened cylindrical shell and the cylindrical shell with two stiffeners positioned at both ends are nearly the same. And also one stiffener positioned at the center makes more contribution to the frequency increase than two stiffeners positioned at both ends. This is an effect of the positions of the ring stiffeners on frequency increase. The fundamental frequency of the cylindrical shell increases as the stiffeners get closer to the center. It keeps increasing up to a critical distance which is z/L=0.3 for the problem considered here. As the ring stiffeners are positioned closer to center than the critical distance, fundamental frequencies start to decrease and converge to the fundamental frequency of the cylindrical shell with one stiffener positioned at the center. Finally when two stiffeners are positioned at the center without any gap between them, the frequency of the cylindrical shell is approximately equal to the frequency of the cylindrical shell with one stiffener positioned at the center. Variations of the fundamental frequencies with the positions of the ring stiffeners for thick and thin cylindrical shells are presented in Figure 5.6.

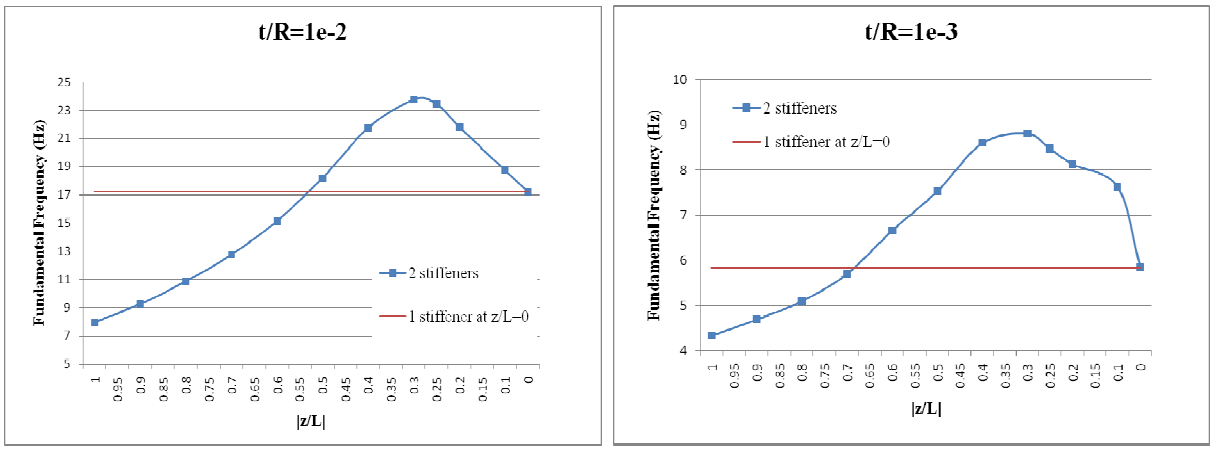

Figure 5.6: Variation of the fundamental frequencies with the positions of the ring stiffeners.

The higher modes of the shell have similar but not exactly the same pattern of increase as the fundamental frequency. Figure 5.4 shows that the frequencies are increasing significantly between two consecutive modes and these increases are not always happening at the same mode for different models. As a result of these differences between models, the highest frequency could be obtained at a different position of the ring support. That makes the variation of the frequencies in higher modes different than the variation of the fundamental frequencies.

For the thin cylindrical shell, two ring stiffeners positioned at both ends of the cylindrical shell make more contribution to the stiffness than they do for the thick cylindrical shell. But we can see in Figure 5.7 that the contribution of two ring stiffeners positioned at both ends is still less than the contribution of one ring stiffener positioned at the center. For the thick cylindrical shell, it is observed that the stiffeners at both ends render nearly no contribution to the stiffness but the same stiffeners contributed more when they were attached to the thin cylindrical shell. The reason of this difference in behavior between the thick and thin cylindrical shells is the effect of the ring stiffeners to the stiffness of the cylindrical shells. The same geometry of ring stiffeners is used for both cylindrical shells and the ring stiffener modeled here is stiffer for the thin shell compared to the thick shell. That is, the bending rigidity of the ring stiffener in its plane is much more rigid compared to the bending rigidity of the shell. So when the ring stiffeners are positioned at both ends of the thin cylindrical shell, they don't deform with the shell. So this is like changing the boundary conditions of a cylindrical shell from simply supported to clamped and it is known that different boundary conditions result in different frequencies for the same geometry of a cylindrical shell [1,4]. So in the case of the thin cylindrical shell the ring stiffeners positioned at both ends increase the frequencies more than the case for the thick cylindrical shell. However the variation pattern of the fundamental frequencies with the position of the stiffeners is similar to that of the thick cylindrical shell and presented in Figure 5.6.

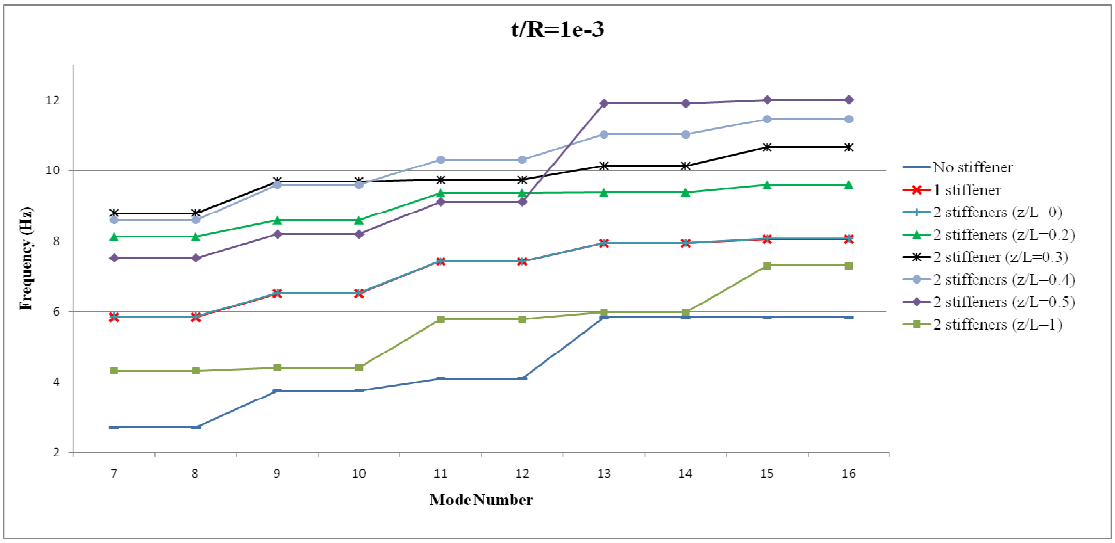

Figure 5.7: The frequencies of the thin cylindrical shell ($t/R=10^{-3}$) at different positions of the ring stiffeners.

5.3.2 Comparison of the study with the literature

It is important to compare the results of the study with an analysis from the literature in order to verify that good results are obtained in this part of the thesis. The analytical solution of free vibration problems of stiffened shells presents considerable difficulties and it is hard to find a general solution that can be applied to all boundary conditions and shell geometries. Among many studies, ref. [4] is chosen because of its similarity to the study carried on here. The results presented in this study are compared with the results presented in [4] considering mostly the qualitative behavior of the results. Loy and Lam [4] have studied the frequencies of cylindrical shells with a ring support. The ring support is arbitrarily placed and it is assumed that the ring stiffeners imposed zero lateral deflection on the model. The governing equations are derived using an energy functional with the Ritz method. The results are obtained by solving the governing equations. A part of the study which is about the influence of the position of the ring stiffener is related to the study carried out in this thesis. In this part, the variation of the fundamental frequency with the position of the ring stiffener for the cylindrical shell with different boundary conditions is studied. In Figure 5.8 dimension parameters of the cylindrical shell are presented. The dimensions of the cylindrical shell are t/R=0.01 and L/R=20. In the solution process it is assumed that the fundamental frequencies are obtained at the mode shape in which the cylindrical shell makes one circumferential full wave and one longitudinal half wave.

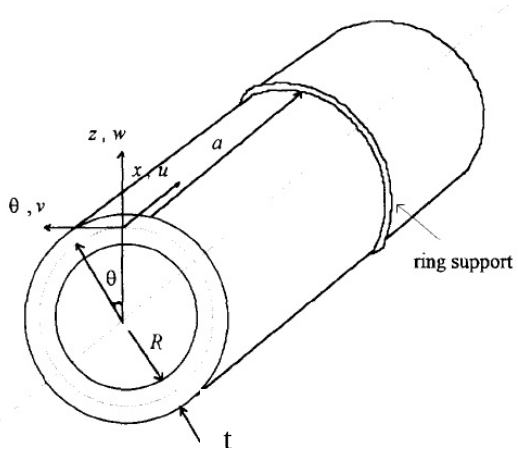

Figure 5.8: The dimension parameters of the cylindrical shell [4]**.**

In [4] the variation of the fundamental frequency with the position of the ring stiffener is studied by using one ring stiffener in the model. In this thesis, two ring stiffeners are used to study the variation of the fundamental frequency. Those stiffeners are positioned symmetric to each other. The reason to model the problem in this way in finite element analysis was to be able to have a similarity in the geometry and boundary conditions between the analytical solution and the finite element solution. So the finite element model can be thought of as two similar cylinders which are connected at the symmetry plane at z=0. Because of this symmetry, one half of the cylindrical shell will be considered when comparing the results of the finite element solution with the analytical solution. The symmetry and similarities lead us to a new cylindrical shell which is obtained by cutting the model considered in this thesis at the symmetry plane and considering one half. In this section, the “half” cylindrical shell will refer to the half of the cylindrical shell modeled in the finite element analysis and the “half” cylindrical shell is presented in Figure 5.9. It is shown that the “half” cylindrical shell is closed with a hemisphere at one end and free at the other. In order to have a similarity with the model used in the analytical solution, these conditions can be thought of as if it is clamped-free at two ends. Of course these conditions are not fully satisfying clamped-free boundary conditions. The results will be compared and interpreted by keeping in mind that there are differences between the two models.

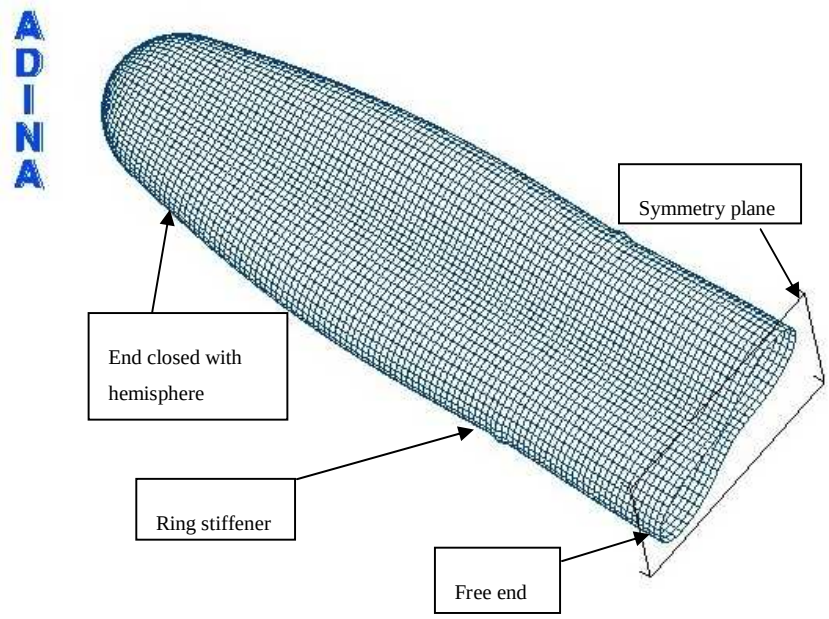

Figure 5.9: The “half” cylindrical shell.

Here it is important to note the differences in the geometry of the model and the assumptions made in the solution process. The differences between the two models should help to explain the differences in the results. The analytical solution [4] is obtained by assuming that the ring stiffeners are imposing zero lateral deflection and the boundary conditions are clamped-free at two ends of the cylinder. But in the finite element model the ring stiffeners are deforming with the shell so they are not imposing zero lateral defections. As mentioned above the boundary conditions are similar but not the same. The effect of the hemisphere can be considered as a clamp but it is obvious that the end closed with the hemisphere is not as stiff as a clamped end. At the symmetry plane the “half” cylindrical shell is free to move in the lateral direction but restricted in the axial direction. This effect can be approximated as a free end. In the analytical solution the dimensions of the cylindrical shell are t/R=0.01 and L/R=20. Since we are considering the “half” cylindrical shell, the dimensions of the finite element model are t/R=0.01 and L/R=10. So we have the same thickness but the “half” cylindrical shell is shorter than the model used in the analytical solution.

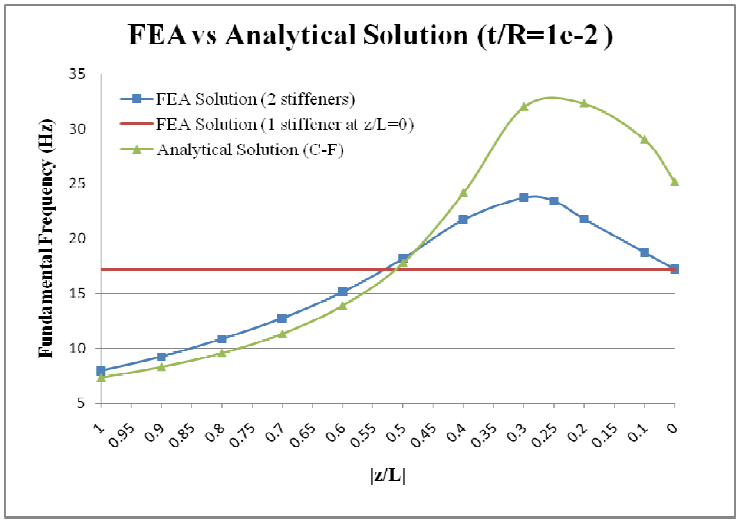

Figure 5.10: Variation of the fundamental frequency with the position of the ring stiffeners.

The results of the analytical solution [4] and the finite element analysis are plotted in Figure 5.10. The variation of the fundamental frequency with the position of the ring stiffener is qualitatively similar for both solutions. The fundamental frequencies are increasing as the ring stiffeners get closer to the free ends of the cylinders (which is the centre of the cylindrical shell in the finite element analysis). The fundamental frequencies are reaching their maximum values at a distance that is approximately one-third of the length from the free end. Beyond the critical distance the fundamental frequencies are decreasing and converging to a value. Although the variation of the fundamental frequency is qualitatively similar for both solutions, it is observed that the fundamental frequencies are different. In Figure 5.10, two curves intersect approximately at z/L=0.5. This distance is half of the distance between clamped and free ends. In the region where the ring stiffener is closer to the clamped end, the results are similar but the fundamental frequencies of the finite element solution are higher. Since the “half” cylindrical shell is shorter than the cylindrical shell used in the analytical solution, it is normal to have higher frequencies in the finite element solution. It is known that the frequencies increase as the cylindrical shell gets shorter [4]. In the region where the ring stiffener is closer to the free end, there is a significant difference in the results. Results of the analytical solution are significantly higher than results of the finite element solution. Although we have a shorter cylindrical shell in the finite element model and it is expected to have higher frequencies for this model, in this region the effect of the ring stiffener overcomes the effect of the length difference. It is assumed that the ring stiffener

imposes zero lateral deflection in the analytical solution and deforms with the shell in the finite element analysis. It can be said that the ring stiffener used in the analytical solution is stiffer than the one used in the finite element analysis. So the contribution of the ring stiffener is different for the two models. This effect cannot be observed in the region where the ring stiffener was closer to the clamped end because the lateral deflection of the cylindrical shell is already restricted by the clamped boundary condition. Figure 5.9 shows that the lateral deflection of the cylindrical shell is increasing with the distance measured from the clamped end. As the ring stiffener gets closer to the free end, the lateral deflection of the cylindrical shell increases and the fact that the ring stiffener is not stiff enough in the finite element model becomes important. So the fundamental frequencies of the analytical solution are higher and that can clearly be seen in Figure 5.10.

5.4 Variation of the Frequencies with the Number of Uniformly Distributed Ring Stiffeners

There is a increase in the frequencies as the stiffeners are added. However, in bending modes there is a very small decrease in the frequencies. The reason is that in bending modes the cylindrical shell makes no circumferential waves and it bends globally. So there is very little bending in the circumferential direction and the stiffeners are not contributing to the stiffness. But they are adding to the inertia of the cylindrical shell and that lowers the frequencies in bending modes [1]. Figures 5.11 and 5.12 present the frequency variation with mode numbers for the cylindrical shells with different numbers of ring stiffeners. It is also seen in the figures that after the bending modes, the frequencies are increasing immediately. The increase is proportional to the number of ring stiffeners. This means that after the bending mode, the cylindrical shell makes circumferential waves and as a result of this bending, the ring stiffeners start to contribute to the stiffness. So the frequencies increase much more after the bending mode if the cylindrical shell has more ring stiffeners.

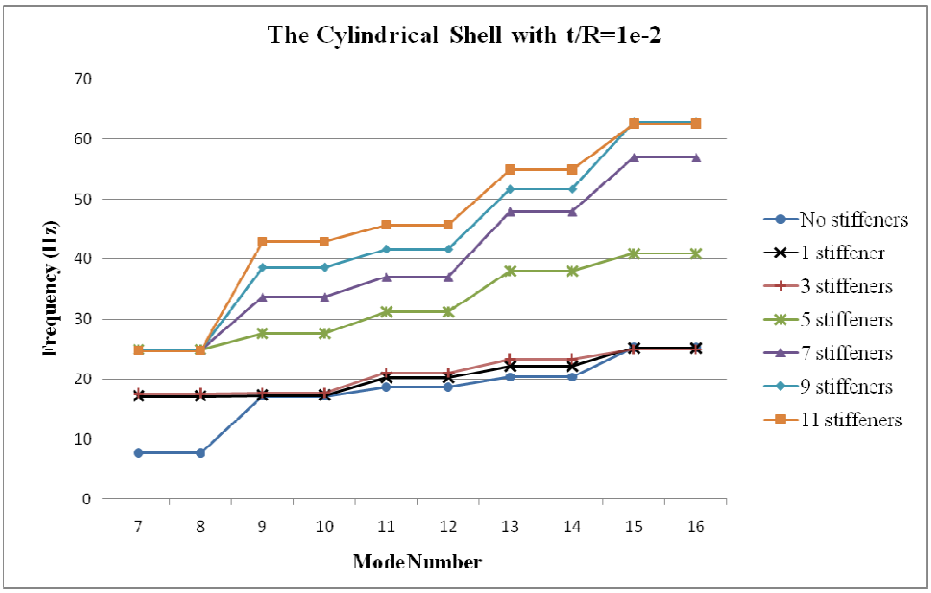

Figure 5.11: The frequencies of the thick cylindrical shell ($t/R=10^{-2}$).

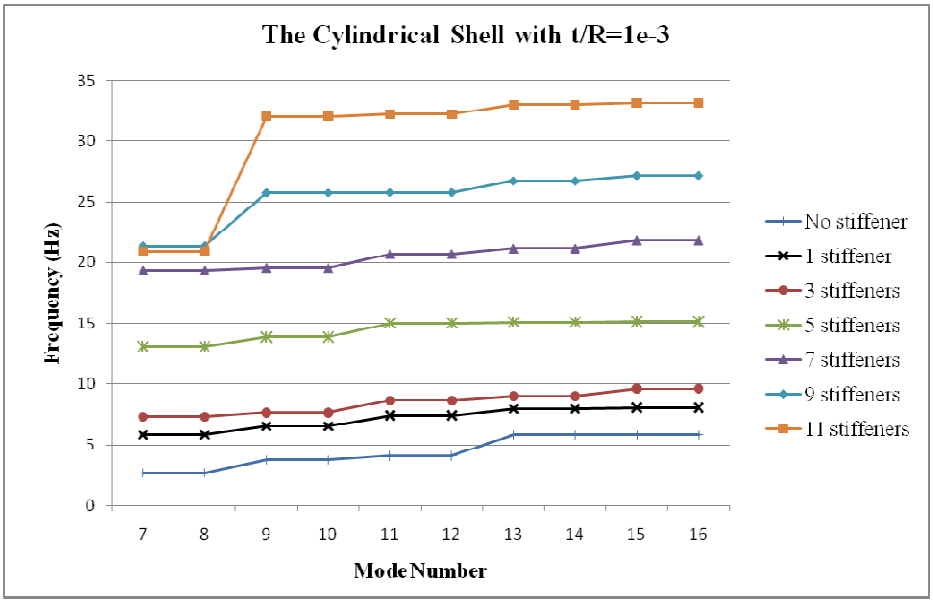

Figure 5.12: The frequencies of the thin cylindrical shell ($t/R=10^{-3}$).

In some modes, the cylindrical shell makes the same number of waves in both directions, and they have different frequencies and mode shapes in those modes. The modes in which this phenomenon is observed have an even number of circumferential waves. The difference of the mode shapes is that the parts of the cylindrical shell corresponding to the half wave in the longitudinal direction are rotated relative to each other. This rotation is around the longitudinal

direction and an example can be seen in Figure 5.13. In Figure 5.13, mode 12 of the thick cylindrical shell with three ring stiffeners is presented. In mode 12, the thick cylindrical shell has two longitudinal half waves and three circumferential full waves. Two longitudinal half waves are making a continuous full sine wave in the longitudinal direction.

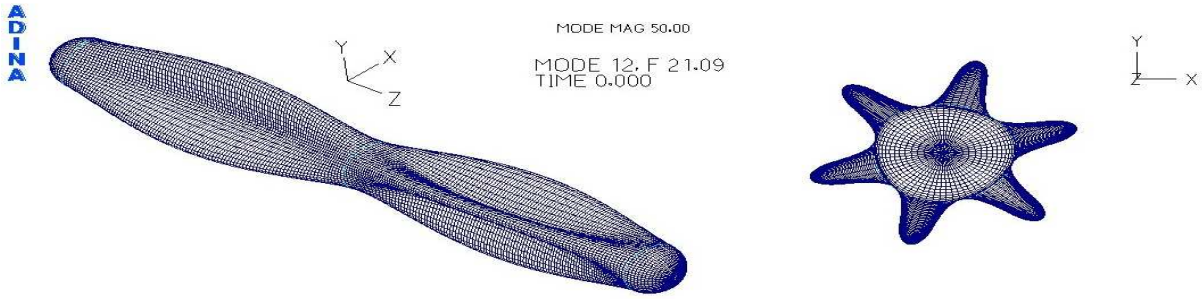

Figure 5.13: Mode 12 of the thick cylindrical shell ($t/R=10^{-2}$).

Mode 13 of the same shape has the same number of waves but the half parts are not rotated and two half sine waves are repeated in the longitudinal direction. The frequency of this mode is higher than the frequency of mode 12. Mode 13 is presented in Figure 5.14. Here, the thick cylindrical shell with three ring stiffeners is presented as an example and its outline is shown in Figure 5.15. Results for the cylindrical shells analyzed in this study show that if two modes have the same number of waves, the one with rotation has a lower frequency. The rotation allows the structure to deform so that it makes a continuous full sine wave in the longitudinal direction. It is thought that having this mode shape is easier for the cylindrical shell since it is an easier way to deform in the longitudinal direction. So this mode shape has a lower frequency than the one in which the shell makes repeated half sine waves.

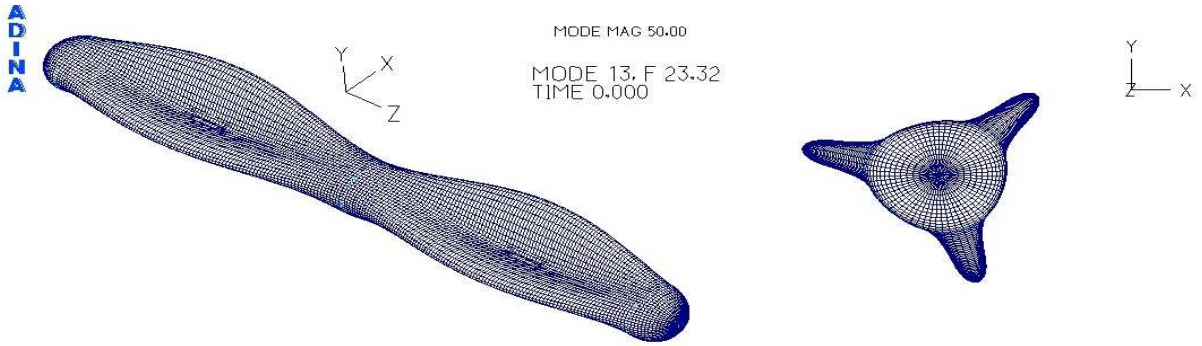

Figure 5.14: Mode 13 of the thick cylindrical shell ($t/R=10^{-2}$).

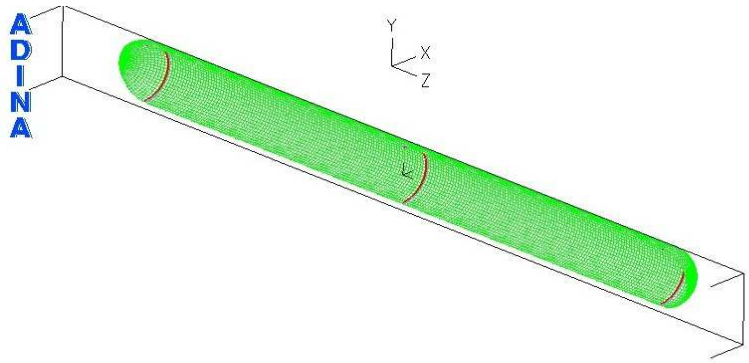

Figure 5.15: Positions of the ring stiffeners for the cylindrical shell with three stiffeners.

For the thick cylindrical shell, the mode shape is always consistent with the mode shape of a single ring stiffener considering the circumferential direction (n=2, 3...). The vibration modes of the ring-stiffened cylindrical shell are very similar to those of the unstiffened cylindrical shell for the lower modes. The ring stiffeners deform consistently with the corresponding mode shape of the cylindrical shell. However, different vibration modes are observed in the higher modes. Especially beyond mode 11, adding ring stiffeners affects the vibration modes of the thick cylindrical shell.

The fundamental modes of the thick cylindrical shell with five and more ring stiffeners are bending modes. That causes the fundamental frequencies to converge. When bending modes exist, the ring stiffeners don't increase the frequencies of the cylindrical shell. The results of the cylindrical shells with five and more stiffeners show that the frequencies converge approximately to 25 Hz. Also the last two modes of the cylindrical shell with nine and eleven stiffeners are bending modes and the frequencies converge approximately to 62 Hz.

In Figure 5.11, it is seen that the frequencies of the unstiffened cylindrical shell, the cylindrical shells with one stiffener and three stiffeners are very close. Despite the existence of two extra stiffeners, there is no significant increase in the frequencies of the cylindrical shell with three stiffeners compared with the cylindrical shell with one stiffener. That can be explained by the effect of the positions of the stiffeners on the frequencies. This subject is discussed in Section 5.3.1. It is known that the contribution of the ring stiffeners positioned at both ends is very limited. In the design of the cylindrical shell with three ring stiffeners there are two ring

stiffeners at both ends and there is a ring stiffener at the center of the cylinder in the longitudinal direction. Also for the shell with one stiffener, the ring stiffener is positioned at the center of the cylinder in the longitudinal direction. Positions of the stiffeners can be seen in Figure 5.15. The contribution of the ring stiffeners positioned at both ends is very limited and a bigger part of the extra stiffness comes from the ring stiffeners positioned at the center. As a result, considering the contribution to the stiffness, the effects of one stiffener and three stiffeners positioned as in Figure 5.15 are approximately the same. Since only one stiffener is contributing to the stiffness of the whole structure, the frequency increase is lower than that of the other designs which are the cylindrical shells with five and more stiffeners.

For the thin cylindrical shell, the ring stiffeners don't deform and they act like constraints at their positions. Since the stiffeners are constraining the shell, it makes longitudinal half waves between them. So globally, the thin cylindrical shell makes "a-1" longitudinal half waves where "a" is the number of ring stiffeners used. We know that the thin unstiffened cylindrical shell makes one longitudinal half wave. As a result of adding ring stiffeners, both the number of longitudinal half waves and of the circumferential full waves increases.

Contrary to the case of the thick cylindrical shell the contribution of the ring stiffeners is approximately constant for the thin cylindrical shell. Since the ring stiffeners are very stiff for the thin cylindrical shell, they dramatically change the mode shapes of the shell. So every ring stiffener contributes to the stiffness of the whole structure and they increase the frequencies. In Figure 5.12, we can see that the increase is approximately constant since two ring stiffeners are added to the previous design at every step. Frequencies of the cylindrical shell with one stiffener and three stiffeners are increased less than those of the other designs. The increase is small because two of the three stiffeners are positioned at both ends of the cylindrical shell and their contribution to the stiffness is still small compared to those of the stiffeners which are positioned closer to center of the cylindrical shell in the longitudinal direction. But the frequencies of the cylindrical shells with one and three stiffeners are not very close to each other as we observed in the case of the thick cylindrical shell. For the thin cylindrical shell, the ring stiffeners positioned at both ends affect the mode shapes contrary the case of the thick cylindrical shell. This effect can be thought of as changing the boundary conditions of a cylindrical shell from simply supported to clamped and it is known that different boundary conditions result in different

frequencies for the same geometry of a cylindrical shell [1,4]. So in the case of the thin cylindrical shell it is observed that the frequency increase is more than that observed for the thick shell when the ring stiffeners are positioned at the ends of the cylinder.

The positions of the stiffeners have a big role in the frequency increase. The cylindrical shell with three stiffeners can be though of as it consisted of cylindrical shells with one stiffener and two stiffeners positioned at both ends, respectively. Keeping that in mind, superposition of two designs gives us an approximate result to find the frequencies of the cylindrical shell with three stiffeners. First, the effect of the ring stiffeners at their particular positions is found. That is, the differences of the frequencies of those cylindrical shells and the unstiffened cylindrical shell are calculated. Then the differences for the cylindrical shell with one stiffener and two stiffeners are added to each other. The results in Table 5.1 shows that the sum of the frequency increase for two separate designs considered here gives an approximate value for the frequency increase of the cylindrical shell with three stiffeners.

Table 5.1: The effect of the ring stiffeners to the frequency increase.

Mode Number	Frequencies (Hz)				Differences in the freq.			Comparison	
	No Stiffener (f0)	1 Stiffener (f1)	2 Stiffeners (f2)	3 Stiffeners (f3)	f1-f0	f2-f0	f3-f0	(f1-f0)+(f2-f0)	f3-f0
7	2.714	5.84	4.316	7.3616	3.126	1.602	4.6476	4.728	4.6476
8	2.714	5.84	4.316	7.3616	3.126	1.602	4.6476	4.728	4.6476
9	3.753	6.521	4.402	7.642	2.768	0.649	3.889	3.417	3.889
10	3.753	6.521	4.402	7.642	2.768	0.649	3.889	3.417	3.889
11	4.093	7.424	5.781	8.648	3.331	1.688	4.555	5.019	4.555
12	4.093	7.424	5.781	8.648	3.331	1.688	4.555	5.019	4.555
13	5.831	7.947	5.979	9.048	2.116	0.148	3.217	2.264	3.217
14	5.831	7.947	5.979	9.048	2.116	0.148	3.217	2.264	3.217
15	5.838	8.062	7.3	9.624	2.224	1.462	3.786	3.686	3.786
16	5.838	8.062	7.3	9.624	2.224	1.462	3.786	3.686	3.786

5.5 Comparison of the Results with the Analytical Solution

The analytical solution for the free vibration of unstiffened cylindrical shell is presented in Section 4.3.1. In Sections 5.3 and 5.4, the cylindrical shell is stiffened with ring stiffeners and the problem is solved using finite element analysis in ADINA. In Section 5.3.2, the results of the

variation of the fundamental frequencies with the position of the ring stiffeners are compared with the results of the analytical solution. In this section the purpose is to compare the finite element solution with the analytical solution to have insight into how two solutions differ and how the assumptions made through the analysis affect the solution.

5.5.1 The analytical solution of the free vibration problem of ring-stiffened cylindrical shells

The analytical solution of the free vibrations of stiffened cylindrical shells presents many difficulties. That leads researchers to solve this problem by approximate methods. The method of an approximate analysis is presented in [16] in detail. The free vibration problem of ring stiffened cylindrical shells is approximated in two ways. The ratio between the flexural stiffness of the ring stiffener in its own plane and the shell itself is used as a reference to choose the appropriate method to solve the problem [16]. If the shell stiffness multiplied by the distance between the ring stiffeners (D. l_x) is significantly less than the flexural stiffness of the ring stiffener (E.I_r), then the natural frequencies can be found using (4.1). That is, if the flexural stiffness of the ring stiffener is significantly more than the stiffness of the shell, then the part between two stiffeners can be isolated and the problem will be solved for this part. In that case the following equation should be used to solve the free vibration problem.

$$\omega^2 = \frac{E}{\rho R^2(1-\nu^2)} \frac{(1-\nu^2)\lambda^4 + a^2(\lambda^2+n^2)^4}{n^2+(\lambda^2+n^2)^2} \tag{5.1}$$

where n is the number of circumferential half waves, m is the number of longitudinal full waves, $\lambda = \frac{m\,\pi R}{l_x}$ and $a^2 = \frac{t^2}{12\,R^2}$.

If the shell stiffness multiplied by the distance between the ring stiffeners (D. l_x) is significantly larger than the flexural stiffness of the ring stiffener (E.I_r), then the stiffness of the ring stiffeners can be uniformly distributed over the shell. The cylindrical shell will be considered structurally orthotropic, which means that it has different flexural stiffness in the longitudinal and the circumferential directions [16]. So the flexural stiffness of the ring stiffeners will be added to the

flexural stiffness of the shell in the circumferential direction. The natural frequencies of the structurally orthotropic cylindrical shell can be calculated by the following equation.

$$\omega^2 = \frac{1}{\rho\, t\, R^2} \frac{\left(\lambda^4 Et + \frac{(D + EI_r/l_x)}{R^2}(\lambda^2 + n^2)^4\right)}{(\lambda^2 + n^2)^2 + n^2} \tag{5.2}$$

where n is the number of circumferential half waves, m is the number of longitudinal full waves, $\lambda = \frac{m\,\pi R}{l_x}$, $a^2 = \frac{t^2}{12\,R^2}$. (5.2) is valid if the material properties of the ring stiffener is the same as or differs slightly from the material properties of the shell. For structures having ring stiffeners with material properties which are different from the shell material properties, (5.2) must be defined again. Detailed information about that kind of formulation is presented in [16].

5.5.2 Comparing the Finite element solution with the analytical solution

In Section 5.4, the cylindrical shells with t/R=10^{-2} and t/R=10^{-3} are stiffened with uniformly distributed ring stiffeners. The natural frequencies of the stiffened cylindrical shells are calculated by finite element analysis. In this part, the finite element solution will be compared with the analytical solution which is mentioned in Section 5.5.1. The comparison is carried out for the "thin" cylindrical shell (t/R=10^{-3}) which is stiffened with three ring stiffeners. The model is presented in Figure 5.16.

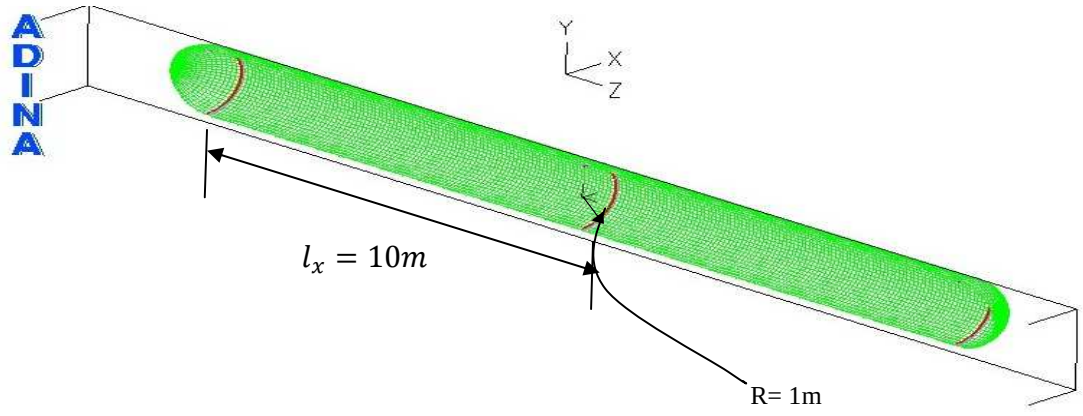

Figure 5.16: The "thin" cylindrical shell with three stiffeners.

As mentioned in Section 5.5.1, first the ratio between the values of (D.l_x) and (E.I_r) should be compared in order to choose the appropriate frequency equation to solve the problem. Using the dimensions and the material properties of the "thin" cylindrical shell and the ring stiffener we obtain the following:

$$D.l_x = \frac{Et^3}{12(1-\nu^2)}.l_x = \frac{210\times10^9.(1\times10^{-3})^3}{12(1-0.3^2)}.10 = 192.3$$
$$E.I_r = E.\left(\frac{bt_r^3}{12}\right) = 210\times10^9.\left(\frac{6.42\times10^{-3}.(16\times10^{-2})^3}{12}\right) = 4.6\times10^5 \quad (5.3)$$

It is obvious that for the "thin" cylindrical shell, (D.l_x) is significantly less than (E.I_r). So it can be concluded that (5.1) is valid to solve this problem. The frequencies of the "thin" cylindrical shell with three stiffeners are calculated using (5.1), assuming that the shell has one longitudinal half wave. The results of the analytical and finite element solutions are plotted in Figure 5.17. As expected, the analytical solution is qualitatively similar to the solution of the unstiffened cylindrical shell. Since one part of the cylinder between the stiffeners is considered in the analytical solution, it is normal to have similar results to those of the unstiffened cylindrical shell.

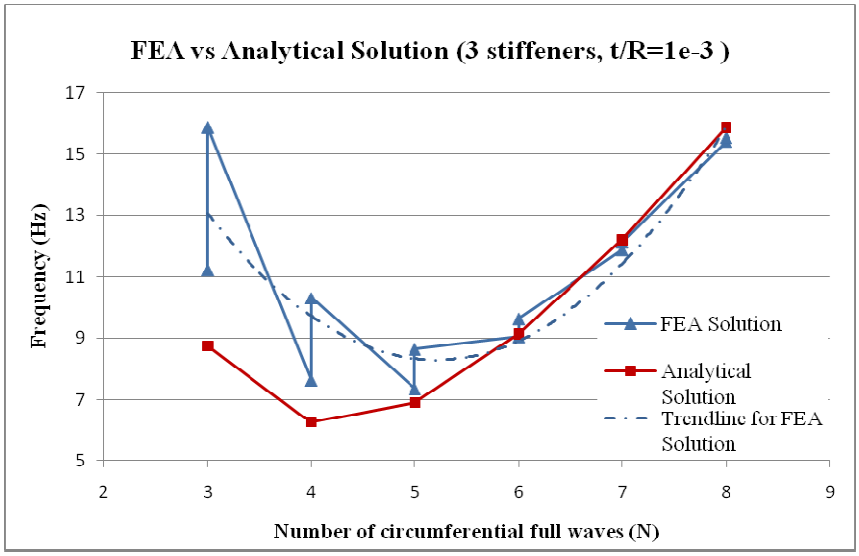

Figure 5.17: The comparison of the results for the "thin" cylindrical shell with three stiffeners.

Another important outcome of this assumption is that the analytical solution cannot predict all of the frequencies which arise for the same number of waves in both directions. The cylindrical shell can have different frequencies for the same number of circumferential and longitudinal waves. Since the analytical solution isolates one part of the cylindrical shell, the frequencies arising from the interaction of the shell parts, whose boundaries are defined by the ring stiffeners, cannot be calculated. In Figure 5.17, the finite element solution has multiple frequencies for one particular number of circumferential waves while the analytical solution has only one for the same number of circumferential waves. Aside from having multiple frequencies for the same number of circumferential waves, the interaction of the shell parts also increases the frequencies. Since the analytical solution assumes that the isolated part of the cylinder is simply supported at both ends, the frequencies are lower than the frequencies of the finite element solution. But it is important to note that beyond six circumferential waves, the two solutions are becoming similar. When the stiffened cylindrical shell makes many circumferential waves, it is hard for it to deflect laterally at the positions of the stiffeners. Then the cylindrical shell acts more like it is simply supported at the positions of the stiffeners. So the finite element solution converges to the analytical solution as the number of circumferential waves increases.

5.6 Conclusions for the Study on the Stiffened Cylindrical Shells

The frequencies and the mode shapes of stiffened cylindrical shells are analyzed. The change of the frequencies with the positions of the ring stiffeners and the change of the frequencies with the number of uniformly distributed ring stiffeners are studied in two separate sections.

The studies show that the ring stiffeners have an important influence on the frequencies and the mode shapes of the cylindrical shells. The frequencies increase with the number of stiffeners when the cylindrical shell takes on circumferential waves. If the shell does not deflect into circumferential waves, which is the case in bending modes, the frequencies decrease slightly when more ring stiffeners are added. Study on the variation of the frequencies with the position of the ring stiffeners showed the importance of the position of the ring stiffeners for the contribution to the stiffness.

The effect of the ring stiffeners on the thick and thin cylindrical shells was different because the same ring stiffeners are used for both shells. The ring stiffeners were stiff for the thin cylindrical shell so they changed the mode shapes dramatically.

6. Concluding Remarks

6.1 Conclusions

A study on the free vibrations of the cylindrical shell structures is presented. This thesis focuses on the free vibration characteristics of the stiffened and unstiffened cylindrical shells. The vibration modes of the unstiffened cylindrical shell are analyzed as the shell thickness decreases under unstressed and pre-stressed conditions. The vibration modes of the unstiffened cylindrical shell are highly affected with the change in the thickness. Especially, the lowest frequency changes approximately by the order of the square root of the thickness change. This can be considered a good result since the unstiffened cylindrical shells studied in this thesis can be considered membrane dominated and it is expected that their lower frequencies be scaled with $\sqrt{t}$. The mode shapes of the cylindrical shell are also affected. As the shell gets thinner, the number of the circumferential waves increases while the number of the longitudinal waves decreases. The initial membrane stresses also change the free vibration modes of the unstiffened cylindrical shell. The tensile stresses make the shell stiffer while the compressive stresses make it softer compared to the unstressed condition. The thin cylindrical shells are more sensitive to the initial stresses than the thick cylindrical shells. An interesting observation is that the initial tensile stresses affect the rigid body rotations and increase the corresponding frequencies which are zero in the unstressed case. The finite element solution is compared with the available analytical solutions from the literature and verified.

The vibration modes of the stiffened cylindrical shell are studied in two parts. In the first part, the influence of the positions of the ring stiffeners on the fundamental frequencies is studied with a cylindrical shell with two stiffeners. Changing the positions of the ring stiffeners along the longitudinal axis of the cylindrical shell affects the fundamental frequencies. As the ring stiffeners are further away from the end closures of the cylindrical shell, the fundamental frequencies increase. In the second part, the free vibration modes of the stiffened cylindrical shell are studied. Two cylindrical shells with different thicknesses are stiffened with different numbers of ring stiffeners which are uniformly distributed along the longitudinal axis of the shell. Adding ring stiffeners increases the frequencies of the cylindrical shell in the vibration modes in which the shell is making circumferential waves. The results are compared with the analytical solutions

and the studies from the literature. Although there were differences in the solutions because of the assumptions made in the analyses, it is seen that the results are qualitatively consistent.

6.2 Recommendations for Further Study

Shell structures, especially cylindrical shells, are widely used in the aerospace and naval architecture industries. Submarine/ship hulls, aircraft/rocket bodies and missiles can be basically idealized as cylindrical shell structures. Those structures can be stiffened with ring stiffeners or stringers according to their area of usage. For example, submarine hulls are mostly ring stiffened while aircraft bodies are stringer stiffened. The choice of the type of stiffener mostly depends on the externally applied loads on the structure. This thesis focused on the free vibrations of the cylindrical shell inspired by the submarine design. Considering the wide usage of cylindrical shells in the industry, further research would be useful to make improvements in the designs of those structures. Some recommendations on further study are the following:

- In this thesis the cylindrical shell is studied with constant material properties. The effect of the material properties on the free vibration modes can be investigated. Also considering the aerospace industry, composite material can be used in the model.
- The effect of the initial stresses is studied only for the unstiffened cylindrical shell. Especially for the stiffened cylindrical shell, the effect of the initial stresses should be studied. For the naval construction industry, the effect of the increasing compressive stresses on the vibration modes can be studied. The correlation between the natural frequencies and the buckling mode of the cylindrical shell could be an interesting field of study.
- In this thesis the cylindrical shells are stiffened with ring stiffeners. In reality, both ring and stringer stiffeners are used to stiffen the cylindrical shells. The cylindrical shell could be stiffened with both type of stiffeners and pre-stressed in the longitudinal and the circumferential directions separately. The role of the stiffeners on the resistance to different kinds of loads could be studied.
- Recent studies in carbon nanotube-based composites give a hint about how thinner shell structures may be constructed in the future. In this thesis the thickness of the cylindrical shell is decreased up to 10^{-5} m. The free vibration behavior of thinner shells could be a useful and necessary study for the future.

Appendix A – A Study on the Free Vibrations of a Truss Element

In Section 4.4 initial tensile stress is applied on the unstiffened cylindrical shell. The results show that the tensile stress affects the rigid body modes of the cylindrical shell. The lowest six frequencies of the unstressed cylindrical shell are zero. However, when initial tensile stress is applied on the shell, the lowest three frequencies remain zero but the 4^{th}, 5^{th} and 6^{th} frequencies of the pre-stressed shell are nonzero. The initial tensile membrane stresses restrict the rigid body rotations of the cylindrical shell. In this section, solution of the free vibration problem of a truss element will be demonstrated in order to study the effect of the initial tensile stress on rigid body modes.

A.1 Formulation of the Finite Element Nonlinear Analysis

The free vibration problem of a pre-stressed truss element is a nonlinear problem. So we need to use nonlinear finite element formulation in order to solve the problem. Detailed discussion of the nonlinear finite element formulation can be found in Chapter 6 of [5].This appendix mostly focuses on the solution of the free vibration problem of a truss element rather than the formulation. So only a brief explanation is given on the equations needed to understand the formulation.

Here we are dealing with a free vibration problem without damping. So the dynamic equilibrium equation should be used to calculate the frequencies and the mode shapes of the truss. The dynamic equilibrium equation without damping is

$$\boldsymbol{M\ddot{U}} + \boldsymbol{KU} = \boldsymbol{R}(t) \tag{A.1}$$

Since we want to solve the free vibration problem, we consider that there is no externally applied load. For the vibration analysis, the solution to (A.1) can be postulated in the form

$$\boldsymbol{U} = \boldsymbol{\phi}\, \sin(\omega t) \tag{A.2}$$

Substituting (A.2) in (A.1) we get the eigenproblem from which the frequencies and the corresponding mode shapes can be determined.

$$\boldsymbol{K\phi} = \omega^2 \boldsymbol{M\phi} \tag{A.3}$$

where $\boldsymbol{K}$ the stiffness matrix, $\boldsymbol{M}$ is the mass matrix, ω is the frequency of the free vibration and $\boldsymbol{\phi}$ is the corresponding mode shape vector. The eigenproblem in (A.3) yields n eigensolutions. The solution contains an eigenvalue which is the square of the frequency of the free vibration (radians/sec) and an eigenvector which is the corresponding mode shape. The following two new matrices are defined to store the *n* eigensolutions:

$$\boldsymbol{\Phi} = [\boldsymbol{\phi}_1, \boldsymbol{\phi}_2, \dots\dots, \boldsymbol{\phi}_n]; \qquad \boldsymbol{\Omega^2} = \begin{bmatrix} \omega_1^2 & & & \\ & \omega_2^2 & & \\ & & \ddots & \\ & & & \omega_n^2 \end{bmatrix} \tag{A.4}$$

Using the matrices in (A.4), we can write *n* solutions to (A.3) as

$$\boldsymbol{K\Phi} = \boldsymbol{M\Phi\Omega^2} \tag{A.5}$$

To solve the eigenproblem in (A.5), first we need to evaluate the stiffness and mass matrices for the truss element.

In the nonlinear analysis of the structures, the *Lagrangian formulation* is adopted and an incremental formulation is employed to solve the problem [5]. In the Lagrangian incremental analysis approach, the equilibrium of the body at time t using the principle of virtual displacements is expressed as

$$\int_{{}^tV} {}^t\tau_{ij}\delta\ {}_te_{ij}d\ {}^tV = {}^t\mathcal{R} \tag{A.6}$$

where ${}^t\tau_{ij}$: Cartesian components of the Cauchy stress tensor;

$\delta_t e_{ij} = \frac{1}{2}\left(\frac{\partial \delta u_i}{\partial {}^t x_j} + \frac{\partial \delta u_j}{\partial {}^t x_i}\right)$: Components of strain tensor corresponding to virtual displacements;

δu_i : Components of virtual displacement vector imposed on configuration at time t;

${}^tV$: Volume at t;

${}^t\mathcal{R}$: The external virtual work.

In (A.6), the left-hand side is the internal virtual work and the right-hand side is the external virtual work. This is the basic equation to be solved in the nonlinear analysis. For an effective analysis of the nonlinear problems, appropriate stress and strain measures need to be employed [5]. So the principle of virtual displacements is expressed in terms of the second Piola-Kirchhoff stresses and the Green-Lagrange strains.

The second Piola-Kirchhoff stresses are defined as[2]

$$ {}^t_0S_{ij} = \frac{{}^0\rho}{{}^t\rho} {}^0_t x_{i,m} \; {}^t\tau_{mn} {}^0_t x_{j,n} \tag{A.7} $$

where ${}^0\rho$, ${}^t\rho$: the mass density at time 0 and t, respectively;

${}^0_t x_{j,n}$: Components of the deformation gradient [5].

The Green-Lagrange strains are defined as

$$ {}^t_0\epsilon_{ij} = \frac{1}{2}({}^t_0u_{i,j} + {}^t_0u_{j,i} + {}^t_0u_{k,i}.\,{}^t_0u_{k,j}) \tag{A.8} $$

where ${}^t_0u_{i,j} = \frac{\partial\, {}^tu_i}{\partial\, {}^0u_j}$ and ${}^tu_i$ is the component of the displacement vector at time t.

In nonlinear analysis, the constitutive relations are nonlinear and the body can undergo large displacements and strains. As a result, an incremental solution must be improved. The total Lagrangian formulation is used to develop a governing linearized equation [5]. In this solution

[2] Here the notation ${}^t_0A_{ij}$ is used to explain that A is measured at time t referring to the initial configuration which is at time 0.

scheme all variables are referred to the initial configuration at time 0. In the total Lagrangian formulation, (A.6) is expressed as

$$\int_{{}_0V} {}_0^tS_{ij}\delta\,{}_0^t\epsilon_{ij}d\,{}^0V = {}^t\mathcal{R} \tag{A.9}$$

In order to obtain the governing linearized equations the incremental decompositions of stresses and strains should be substituted in (A.9). The incremental decompositions of stresses and strains can be defined as

$$\begin{gathered} {}_o^{t+\Delta t}S_{ij} = {}_o^tS_{ij} + {}_oS_{ij} \\ {}_0^{t+\Delta t}\epsilon_{ij} = {}_0^t\epsilon_{ij} + {}_0\epsilon_{ij};\quad {}_0\epsilon_{ij} = {}_0e_{ij} + {}_0\eta_{ij} \end{gathered} \tag{A.10}$$

In (A.10) the incremental strain is defined as sum of the linear strain increment and the nonlinear strain increment. The linear and nonlinear strain increments are

$$\begin{gathered} {}_0e_{ij} = \frac{1}{2}({}_0u_{i,j} + {}_0u_{j,i} + {}_0^tu_{k,i}.\,{}_0u_{k,j} + {}_0u_{k,i}.\,{}_0^tu_{k,j}) \\ {}_0\eta_{ij} = \frac{1}{2}\,{}_0u_{k,i}.\,{}_0u_{k,j} \end{gathered} \tag{A.11}$$

respectively. Considering (A.9) at time t+Δt and substituting (A.10) and (A.11) in (A.9), we obtain the linearized equations of motion about the state at time t in the total Lagrangian formulation.

$$\int_{{}_0V} {}_0C_{ijrs}\;{}_0e_{rs}\delta\;{}_0e_{ij}d\,{}^0V + \int_{{}_0V} {}_0^tS_{ij}\,\delta\;{}_0\eta_{ij}d\,{}^0V = {}^{t+\Delta t}\mathcal{R} - \int_{{}_0V} {}_0^tS_{ij}\,\delta\;{}_0e_{ij}d\,{}^0V \tag{A.12}$$

In (A.12), ${}_0C_{ijrs}$ is the incremental stress-strain tensor at time t referred to the configuration at time 0 and the remaining terms are discussed in the preceding paragraphs of this chapter.

In the beginning of this chapter, the eigenvalue problem for the free vibration analysis was presented. Now considering the nonlinear effects (A.3) becomes

$$({}_0^t\boldsymbol{K_L} + {}_0^t\boldsymbol{K_{NL}})\boldsymbol{\phi} = \omega^2\boldsymbol{M}\boldsymbol{\phi} \tag{A.13}$$

where ${}_0^t\boldsymbol{K_L}$, ${}_0^t\boldsymbol{K_{NL}}$ are the linear strain incremental and the nonlinear strain incremental stiffness matrices, respectively. They compose the total stiffness matrix. The definition of the mass matrix and the relation between the integrals in (A.12) and the matrices in (A.13) are in the following:

$$\begin{aligned}
&\int_{{}_0V} {}_0C_{ijrs}\ {}_0e_{rs}\delta\ {}_0e_{ij} d\ {}^0V \qquad && {}_0^t\boldsymbol{K_L}\hat{\boldsymbol{u}} = (\int_{{}_0V} {}_0^t\boldsymbol{B}_L^T\ {}_0\boldsymbol{C}\ {}_0^t\boldsymbol{B}_L\ d\ {}^0V)\hat{\boldsymbol{u}} \\
&\int_{{}_0V} {}_0^tS_{ij}\ \delta\ {}_0\eta_{ij} d\ {}^0V \qquad && {}_0^t\boldsymbol{K_{NL}}\hat{\boldsymbol{u}} = (\int_{{}_0V} {}_0^t\boldsymbol{B}_{NL}^T\ {}_0^t\boldsymbol{S}\ {}_0^t\boldsymbol{B}_{NL} d\ {}^0V)\hat{\boldsymbol{u}} \\
& && \boldsymbol{M} = \int_{{}_0V} {}^0\rho\boldsymbol{H}^T\boldsymbol{H} d\ {}^0V
\end{aligned} \tag{A.14}$$

where ${}_0^t\boldsymbol{B}_L$, ${}_0^t\boldsymbol{B}_{NL}$ are the linear and nonlinear strain-displacement transformation matrices respectively, $\boldsymbol{H}$ is the displacement interpolation matrix and $\hat{\boldsymbol{u}}$ is the vector of virtual nodal displacements.

A.2 Free Vibration Problem of a Truss Element

In Section A.1, the finite element nonlinear analysis and the free vibration analysis are summarized and the necessary equations are presented. Now we consider a truss element with two nodes and solve the free vibration problem of it. The two node truss element is shown in Figure A.1.

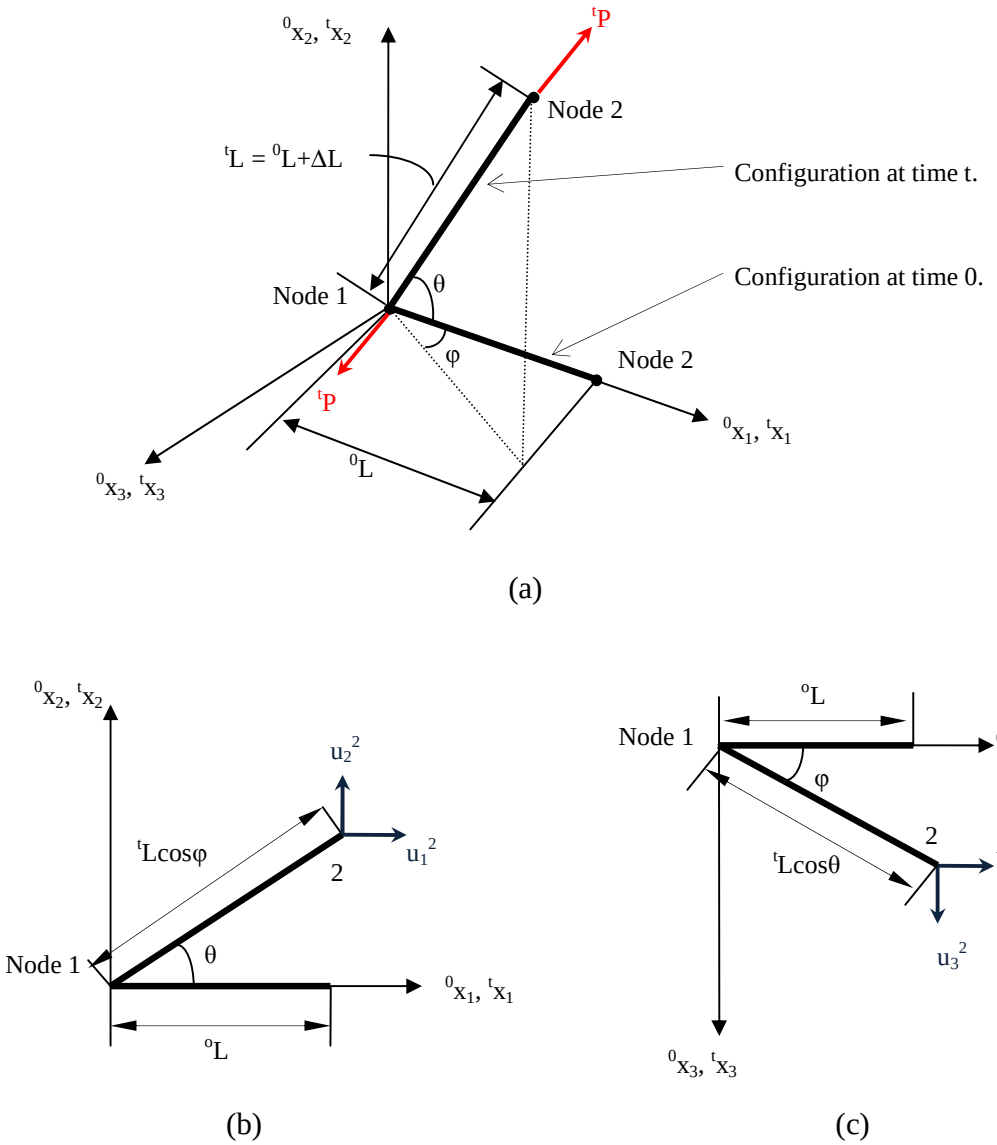

Figure A.1: Two node truss element.

The truss element is straight and aligned with $^0x_1$-axis at time 0. The total Lagrangian formulation will be used to solve the problem. Since the truss is a one dimensional structure the formulation is somewhat simpler than we obtained in the Section A.1. Considering large strain and displacement conditions, first the linear and nonlinear strain increments given in (A.11) should be expressed for our problem. For the truss element we have

$$ {}_0e_{11} = \frac{1}{2}\left({}_0u_{1,1} + {}_0u_{1,1} + {}^t_0u_{k,1}.\ {}_0u_{k,1} + {}_0u_{k,1}.\ {}^t_0u_{k,1}\right);\quad k = 1,2,3 $$

(A.15)

$$ {}_0e_{11} = \frac{\partial u_1}{\partial\ {}^0x_1} + \frac{\partial\ {}^tu_1}{\partial\ {}^0x_1}.\frac{\partial u_1}{\partial\ {}^0x_1} + \frac{\partial\ {}^tu_2}{\partial\ {}^0x_1}.\frac{\partial u_2}{\partial\ {}^0x_1} + \frac{\partial\ {}^tu_3}{\partial\ {}^0x_1}.\frac{\partial u_3}{\partial\ {}^0x_1} $$

$$ {}_0\eta_{11} = \frac{1}{2}\left[\left(\frac{\partial u_1}{\partial\ {}^0x_1}\right)^2 + \left(\frac{\partial u_2}{\partial\ {}^0x_1}\right)^2 + \left(\frac{\partial u_3}{\partial\ {}^0x_1}\right)^2\right] \tag{A.16} $$

Because of the simplicity of the truss geometry here the displacements and the differentials will be obtained by the geometrical relations. Hence we have

$$ \frac{\partial u_1}{\partial\ {}^0x_1} = \frac{1}{{}^0L}[-1 \quad 0 \quad 0 \quad 1 \quad 0 \quad 0][u_1^1 \quad u_2^1 \quad u_3^1 \quad u_1^2 \quad u_2^2 \quad u_3^2]^T $$

$$ \frac{\partial u_2}{\partial\ {}^0x_1} = \frac{1}{{}^0L}[0 \quad -1 \quad 0 \quad 0 \quad 1 \quad 0][u_1^1 \quad u_2^1 \quad u_3^1 \quad u_1^2 \quad u_2^2 \quad u_3^2]^T $$

$$ \frac{\partial u_3}{\partial\ {}^0x_1} = \frac{1}{{}^0L}[0 \quad 0 \quad -1 \quad 0 \quad 0 \quad 1][u_1^1 \quad u_2^1 \quad u_3^1 \quad u_1^2 \quad u_2^2 \quad u_3^2]^T $$

(A.17)

$$ \frac{\partial\ {}^tu_1}{\partial\ {}^0x_1} = \frac{{}^tL\cos\varphi\cos\theta}{{}^0L} - 1;\qquad \frac{\partial\ {}^tu_2}{\partial\ {}^0x_1} = \frac{{}^tL\cos\varphi\sin\theta}{{}^0L}; $$

$$ \frac{\partial\ {}^tu_3}{\partial\ {}^0x_1} = \frac{{}^tL\cos\theta\sin\varphi}{{}^0L} $$

Using (A.17) in (A.15), we therefore have

$$
\begin{aligned}
{}_0e_{11} = \frac{1}{{}^0L}\Bigg\{ & [-1 \quad 0 \quad 0 \quad 1 \quad 0 \quad 0] + \left(\frac{{}^tL\cos\theta\cos\varphi}{{}^0L} - 1\right)[-1 \quad 0 \quad 0 \quad 1 \quad 0 \quad 0] \\
& + \left(\frac{{}^tL\,cos\,\varphi\,sin\,\theta}{{}^0L}\right)[0 \quad -1 \quad 0 \quad 0 \quad 1 \quad 0] \\
& + \left(\frac{{}^tL\cos\theta\sin\varphi}{{}^0L}\right)[0 \quad 0 \quad -1 \quad 0 \quad 0 \quad 1]\Bigg\}\begin{bmatrix} u_1^1 \\ u_2^1 \\ u_3^1 \\ u_1^2 \\ u_2^2 \\ u_3^2 \end{bmatrix}
\end{aligned} \tag{A.18}
$$

$$
{}_0e_{11} = \frac{{}^tL}{\left({}^0L\right)^2}[-\cos\theta\cos\varphi \quad -cos\,\varphi\,sin\,\theta \quad -\cos\theta\sin\varphi \quad \cos\theta\cos\varphi \quad cos\,\varphi\,sin\,\theta \quad \cos\theta\sin\varphi]\begin{bmatrix} u_1^1 \\ u_2^1 \\ u_3^1 \\ u_1^2 \\ u_2^2 \\ u_3^2 \end{bmatrix} \tag{A.19}
$$

From (A.19) we obtain

$$
\boldsymbol{B}_L = \frac{{}^tL}{\left({}^0L\right)^2}[-\cos\theta\cos\varphi \quad -cos\,\varphi\,sin\,\theta \quad -\cos\theta\sin\varphi \quad \cos\theta\cos\varphi \quad cos\,\varphi\,sin\,\theta \quad \cos\theta\sin\varphi] \tag{A.20}
$$

Using the same approach, the nonlinear strain displacement matrix will be obtained. From the relation given in (A.14) the nonlinear strain displacement matrix is

$$
{}^t_0\boldsymbol{B}_{NL} = \frac{1}{{}^0L}\begin{bmatrix} -1 & 0 & 0 & 1 & 0 & 0 \\ 0 & -1 & 0 & 0 & 1 & 0 \\ 0 & 0 & -1 & 0 & 0 & 1 \end{bmatrix} \tag{A.21}
$$

Now that the linear and nonlinear strain displacement matrices have been obtained, the stiffness matrices can be composed substituting (A.20, A.21) in (A.14). The stiffness matrices are

$$ {}_0^t\boldsymbol{K}_L = {}_0C_{1111}\frac{\left({}^tL\right)^2}{\left({}^0L\right)^3}\,{}^0A \ldots $$

$$ \begin{bmatrix} c^2\theta.c^2\varphi & c\theta.c^2\varphi.s\varphi & c^2\theta.c\varphi.s\varphi & -c^2\theta.c^2\varphi & -c^2\varphi.c\theta.s\varphi & -c^2\theta.c\varphi.s\theta \\ & c^2\varphi.s^2\theta & c\theta.c\varphi.s\theta.s\varphi & -c^2\varphi.c\theta.s\varphi & -c^2\varphi.s^2\theta & -c\varphi.c\theta.s\varphi.s\theta \\ & & c^2\theta.s^2\varphi & -c^2\theta.c\varphi.s\theta & -c\varphi.c\theta.s\varphi.s\theta & -c^2\theta.s^2\varphi \\ & & & c^2\theta.c^2\varphi & c^2\varphi.c\theta.s\theta & c^2\theta.c\varphi.s\varphi \\ & Symmetric & & & c^2\varphi.s^2\theta & c\varphi.c\theta.s\varphi.s\theta \\ & & & & & c^2\theta.s^2\varphi \end{bmatrix} \quad \text{(A.22)} $$

$$ {}_0^t\boldsymbol{K}_{NL} = \frac{{}^tP}{{}^tL}\begin{bmatrix} 1 & 0 & 0 & -1 & 0 & 0 \\ 0 & 1 & 0 & 0 & -1 & 0 \\ 0 & 0 & 1 & 0 & 0 & -1 \\ -1 & 0 & 0 & 1 & 0 & 0 \\ 0 & -1 & 0 & 0 & 1 & 0 \\ 0 & 0 & -1 & 0 & 0 & 1 \end{bmatrix} \quad \text{(A.23)} $$

where c(α)=cos(α), s(α)=sin(α) and ${}_0C_{1111} = E$ (Young's modulus). So we obtain the total stiffness matrix adding (A.22) to (A.23). It is important to note that the linear strain stiffness matrix in (A.22) is dependent of the angles θ and φ, while the nonlinear strain stiffness matrix in (A.23) is independent of the angles. The linear strain stiffness matrix accounts for the additional straining of the element and it is dependent of the position of the element at time t. The nonlinear strain stiffness matrix accounts for the effect of the internal stresses/forces which already exist. We also need to compose the mass matrix to complete the matrices to be used in the free vibration equation. The displacement interpolation matrix and the mass matrix for the two node truss element is

$$ \boldsymbol{H} = \begin{bmatrix} \left(1-\frac{{}^0x_1}{{}^0L}\right) & 0 & 0 & \frac{{}^0x_1}{{}^0L} & 0 & 0 \\ 0 & \left(1-\frac{{}^0x_1}{{}^0L}\right) & 0 & 0 & \frac{{}^0x_1}{{}^0L} & 0 \\ 0 & 0 & \left(1-\frac{{}^0x_1}{{}^0L}\right) & 0 & 0 & \frac{{}^0x_1}{{}^0L} \end{bmatrix} \quad \text{(A.24)} $$

$$\boldsymbol{M} = {}^{0}\rho\ {}^{0}A \begin{bmatrix} {}^{0}L/3 & 0 & 0 & {}^{0}L/6 & 0 & 0 \\ 0 & {}^{0}L/3 & 0 & 0 & {}^{0}L/6 & 0 \\ 0 & 0 & {}^{0}L/3 & 0 & 0 & {}^{0}L/6 \\ {}^{0}L/6 & 0 & 0 & {}^{0}L/3 & 0 & 0 \\ 0 & {}^{0}L/6 & 0 & 0 & {}^{0}L/3 & 0 \\ 0 & 0 & {}^{0}L/6 & 0 & 0 & {}^{0}L/3 \end{bmatrix} \tag{A.25}$$

To solve the problem the following geometry and material properties are considered.

- Young's modulus, E=210 GPa;
- The mass density, ${}^{0}\rho$=7,870 kg/m^3;
- Length of the truss at time 0, ^{0}L=3 m.; length of the truss at time t, ^{0}L=3.01 m.;
- The cross-sectional area of the truss, ^{0}A=0.001 m^2;
- The angles at time t, $\varphi=\pi/3$ and $\theta=\pi/6$;
- The tensile force applied on the truss, P= 1x10^6 N.

Using the given values for the geometry and material properties and substituting (A.22, A. 23) and (A.25) in (A.13), we obtain the eigenvalue problem for the free vibration of the truss element. (A.13) is solved for $\boldsymbol{\Phi}$ and $\boldsymbol{\Omega^2}$ under unstressed and pre-stressed conditions of the truss element[3]. The solution for the unstressed truss element is

$$\boldsymbol{\Omega}^2_{\text{UNST}} = \begin{bmatrix} 0 & & & & & \\ & 0 & & & & \\ & & 0 & & & \\ & & & 0 & & \\ & & & & 0 & \\ & & & & & 2.91 \times 10^7 \end{bmatrix} \tag{A.26}$$

$$\boldsymbol{\Phi}_{\text{UNST}} = \begin{bmatrix} -0.2130 & -0.2567 & 0.1046 & -0.0063 & 0.1337 & -0.1712 \\ -0.0895 & 0.1993 & 0.3088 & 0.0193 & -0.1272 & -0.0989 \\ 0.2400 & -0.0551 & -0.0284 & 0.1197 & -0.0756 & -0.2966 \\ 0.3081 & 0.0159 & 0.1398 & -0.1590 & -0.0098 & 0.1712 \\ 0.1012 & -0.0248 & -0.0812 & 0.2093 & 0.3136 & 0.0989 \\ -0.1245 & -0.1377 & 0.0812 & 0.1445 & -0.1397 & 0.2966 \end{bmatrix}$$

[3] The term unstressed expresses that the applied stress ^{t}P is zero and the term pre-stressed expresses that the applied stress ^{t}P is nonzero.

The solution for the pre-stressed truss element is

$$\boldsymbol{\Omega}^2_{\text{STRS}} = \begin{bmatrix} 0 & & & & & \\ & 0 & & & & \\ & & 0 & & & \\ & & & 1.69 \times 10^5 & & \\ & & & & 1.69 \times 10^5 & \\ & & & & & 2.91 \times 10^7 \end{bmatrix} \tag{A.27}$$

$$\boldsymbol{\Phi}_{\text{STRS}} = \begin{bmatrix} 0.0611 & 0.1962 & -0.0110 & 0.2314 & 0.2102 & -0.1712 \\ -0.0690 & 0.0106 & -0.1936 & 0.1873 & -0.2867 & -0.0989 \\ 0.1840 & -0.0611 & -0.0689 & -0.1960 & -0.0258 & -0.2966 \\ 0.0611 & 0.1962 & -0.0110 & -0.2314 & -0.2102 & 0.1712 \\ -0.0690 & 0.0106 & -0.1936 & -0.1873 & 0.2867 & 0.0989 \\ 0.1840 & -0.0611 & -0.689 & 0.1960 & 0.0258 & 0.2966 \end{bmatrix}$$

The results show that the unstressed truss has five zero frequencies and only one nonzero frequency. That means that the unstressed truss element has five rigid body modes. The rigid body modes can also be observed in the eigenvector matrix presented in (A.26). Furthermore the pre-stressed truss element has three zero and three nonzero frequencies which expresses that the pre-stressed truss element has three rigid body modes. It is clear that applying stress on the truss element reduces the number of rigid body modes for deformation-independent loading. Studying the mode shapes of the unstressed and pre-stressed truss elements show that the rigid body rotations are restricted when the stress is applied.

The nonlinear formulation and the free vibration problem presented for the truss element is an important insight to conceptually understand the free vibration analysis of the pre-stressed cylindrical shell presented in Section 4.4. The pre-stressed cylindrical shell has the rigid body modes but its frequencies corresponding to rigid body rotations are very small, because of the effect of the initial loading which is assumed deformation independent. The truss example is presented to express the effect of the deformation independent loading on the frequencies and rigid body modes.

Appendix B - Calculating the Moment of Inertia of Beam Cross Sections

In Chapter 5, ring stiffeners are used to stiffen the cylindrical shell. The ring stiffeners are modeled as curved beams in the finite element analysis. In ADINA, iso-beam elements are used to model the curved beams and the iso-beam elements have rectangular cross-sections. The cylindrical shell model considered in this thesis can be related to a submarine. So the dimensions of the model are chosen by studying the dimensions of submarines. The stiffeners used in the submarines have T cross sections. Since the iso-beam elements have rectangular cross-sections we have to calculate the dimensions of the rectangular cross-section to have equivalent rigidity to that of the T cross-section. The dimensions of the T cross-section are listed in Table B.1 and shown in Figure B.1. Figure B.1.a presents the T cross-section and Figure B.1.b presents the rectangular cross-section.

Table B.1: The dimensions of the beam with T cross-section.

Segment of the T cross-section	**Dimensions**[4]
Flange width (b_f)	5.t
Flange thickness (t_f)	0.375× t
Web height (h_w)	16.t
Web thickness (t_w)	0.375× t

To find the equivalent dimensions for the beam with rectangular cross-section so that its moment of inertia is equal to that of the beam with T cross section, the moment of inertia of the beam with T cross section (I_T) should be evaluated. In this study the moments of inertia of the beams will be calculated about their neutral axes. The coordinate system and the variables to be used are presented in Figure B.2.

[4] Here dimensions are presented proportional to the thickness of the shell (t) used in the model.

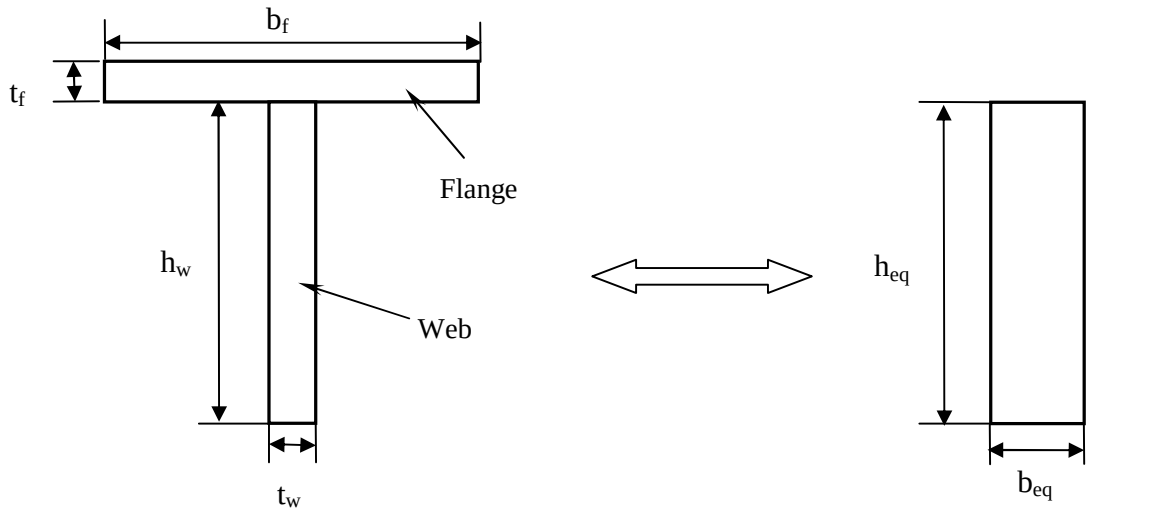

(a) T cross-section

(b) Rectangular cross-section

Figure B.1: The cross sections of the beams used as ring stiffeners.

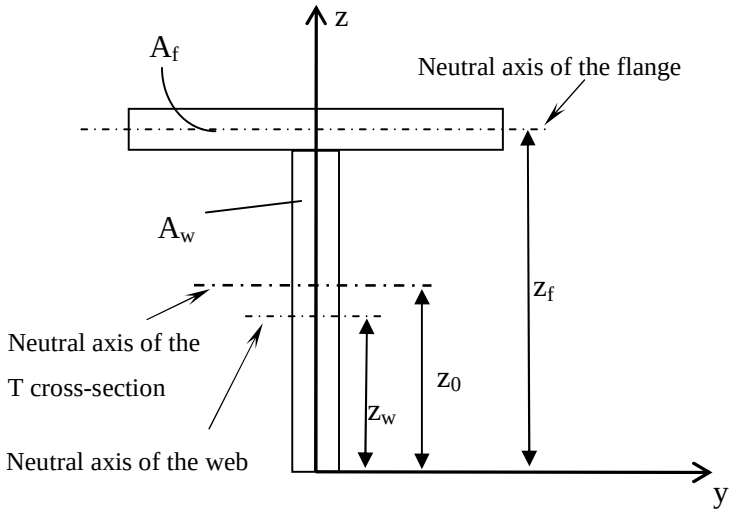

Figure B.2: The coordinate system and the neutral axis of the cross section**.**

First we need to calculate the position of the neutral axis (z_0) of the beam with T cross section from vanishing of the first moment of inertia [6]:

$$\int_A (z - z_0)dA = 0; \qquad \int_{A_w} (z_w - z_0)\, dA_w + \int_{A_f} \left(z_f - z_0\right) dA_f = 0 \tag{B.1}$$

where z_w, z_f are the distances of the neutral axes of the web and the flange from z-axis and A_w, A_f are the areas of the web and the flange, respectively. We therefore have

$$\int_0^{h_w} (z_w - z_0)\, t_w dz_w + \int_{h_w}^{h_w + t_f} \left(z_f - z_0\right) b_f dz_f = 0$$

$$\left(\frac{t_w h_w^2}{2} - h_w t_w z_0\right) + \left(\frac{b_f\left(2h_w t_f + t_f^2\right)}{2} - b_f t_f z_0\right) = 0 \tag{B.2}$$

$$z_0 = \frac{t_w h_w^2 + b_f\left(2h_w t_f + t_f^2\right)}{2(h_w t_w + b_f t_w)}$$

Since $t_f \ll b_f, h_w$, the higher order term of t_f is dropped out. Hence we have the expression

$$z_0 = \frac{t_w h_w^2 + 2b_f h_w t_f}{2(h_w t_w + b_f t_w)} \tag{B.3}$$

for the position of the neutral axis for the beam with T cross-section. Now the moment of inertia can be evaluated. The moment of inertia of a cross-sectional area is defined as [6]

$$I = \int_A (z - z_0)^2 dA \tag{B.4}$$

For the beam with T cross-section, using (B.4) we have

$$I_T = \int_{A_w} (z_w - z_0)^2\, dA_w + \int_{A_f} \left(z_f - z_0\right)^2 dA_f \tag{B.5}$$

Substituting (B.3) in (B.5) and performing the integrals we obtain

$$I_T = \frac{t_w h_w^3}{3} - \frac{t_w h_w^3 + b_f t_f h_w^2}{4\left(1 + \frac{b_f t_f}{h_w t_w}\right)^2} \tag{B.6}$$

To have flexibility through calculations between the real model and the finite element model, the moment of inertia (B.6) will be defined in terms of the shell thickness (t). Using the relations listed in Table B.1, the moment of inertia of the beam with T cross-section is defined as

$$I_T = 219.4 \times t^4 \tag{B.7}$$

We want to have a beam with rectangular cross section which has the same moment of inertia as that of the beam with T cross-section. The moment of inertia for the rectangular cross section is [6]

$$I_R = \frac{bh^3}{12} \tag{B.8}$$

where b is the width and h is the height of the beam. So from (B.7) and (B.8) we obtain

$$I_T = I_R; \qquad \frac{b_{eq} h_{eq}^3}{12} = 219.4 \times t^4 \tag{B.9}$$

Using the same relation given in Table B.1 for the height of the beam, the dimensions of the beam with rectangular cross-section in terms if the shell thickness are obtained as

$$h_{eq} = 16 \times t$$
$$b_{eq} = 0.642 \times t \tag{B.10}$$

As mentioned in Chapter 5, the cylindrical shell with t =10^{-2} is considered to model the ring stiffeners. So the dimensions of the cross-section of the iso-beam which is modeling the ring stiffeners are

$$h_{eq} = 16.10^{-2}\ m$$
$$b_{eq} = 0.642 \times 10^{-2}\ m \tag{B.11}$$

Now that the equivalent dimensions of the rectangular cross-section have been calculated considering the rigidity, it is important to note that the mass of the stiffeners should also be adjusted since we are using different dimensions in our model. The difference in the dimensions results in a difference in the volume of the stiffeners, and of course considering the same density in both models, we obtain different masses. The mass of a single stiffener with T cross-section is

$$M_T = \rho(A_w + A_f)2\pi R \tag{B.12}$$

The mass of a single stiffener with rectangular cross-section is

$$M_R = \rho b_{eq} h_{eq} 2\pi R \tag{B.13}$$

The mass of the cylindrical shell is

$$M_S = M_{cylinder} + 2M_{hemisphere} = \rho t(2\pi R 2L + 4\pi R^2) \tag{B.14}$$

Substituting the numerical values in (B.12-B.14) we obtain

$$M_T = 38.9\ kg;\ \ M_R = 50.7\ kg;\ \ M_S = 10{,}878\ kg \tag{B.15}$$

Total masses of the two models are

$$M_{total}^{R} = s.M_R + M_S;\;\; M_{total}^{T} = s.M_T + M_S \tag{B.16}$$

where $M_{total}^{R}, M_{total}^{T}$ are the total masses of the whole structures stiffened with rectangular and T cross-sectioned stiffeners, respectively and s is the number of stiffeners used in the structure. Here the error is defined as

$$E(\%) = \frac{M_{total}^{R} - M_{total}^{T}}{M_{total}^{R}}.100 \tag{B.17}$$

Now using (B.16) and (B.17), for the cylindrical shell with only one stiffener we have

$$E_1(\%) = \frac{10{,}928.7 - 10{,}916.9}{10{,}928.7}.100 = 0.1\% \tag{B.18}$$

and for the cylindrical shell with 11 stiffeners we have

$$E_{11}(\%) = \frac{11{,}435.7 - 11{,}305.9}{11{,}435.7}.100 = 1.1\% \tag{B.19}$$

In (B.19) the error coming from the difference in the masses for the cylindrical shell with 11 stiffeners is calculated as 1.1%. This is the biggest error for our models because in this thesis the cylindrical shells are stiffened with 11 stiffeners at most. And the error is even smaller for other models analyzed. So it is concluded that this error can be ignored, and mass densities are not adjusted.

Appendix C - Detailed Results of the Free Vibration Modes of the Stiffened Cylindrical Shell

In the following, detailed results are presented for the analyses on free vibration modes of the stiffened cylindrical shell.

C.1 Results for the variation of the frequencies with the position of the ring stiffeners

In the tables "*n*" is the number of circumferential full waves and "*m*" is the number of longitudinal half waves. The parameter defining the position of the ring stiffener (z/L) is presented in Figure 5.5. Some values of *m* are represented by two numbers which one of them is in parentheses. The number in parentheses represents very small half waves between two stiffeners. This distinction is used because those half waves were considerably small when compared to other half waves existing in the same mode shape. And they usually occurred when two stiffeners got very close to each other or to the ends of the cylinder.

Table C.1: The frequencies of the cylindrical shells with 1 stiffener and 2 stiffeners at z/L=0.

Mode Number	1 Stiffener						2 Stiffeners (z/L=0)					
	t/R=1e-2			t/R=1e-3			t/R=1e-2			t/R=1e-3		
	Freq. (Hz)	n	m	Freq. (Hz)	n	m	Freq. (Hz)	n	m	Freq. (Hz)	n	m
1	Rigid body motions.			Rigid body motions.			Rigid body motions.			Rigid body motions.		
2												
3												
4												
5												
6												
7	17.21	2	2	5.84	4	2	17.21	2	2	5.859	4	2
8	17.21	2	2	5.84	4	2	17.21	2	2	5.859	4	2
9	17.36	2	1	6.52	5	2	19.79	2	1	6.535	5	2
10	17.36	2	1	6.52	5	2	19.79	2	1	6.535	5	2
11	20.29	3	2	7.424	5	2	20.29	3	2	7.424	5	2
12	20.29	3	2	7.424	5	2	20.29	3	2	7.424	5	2
13	22.15	3	2	7.947	4	2	22.2	3	2	7.948	4	2
14	22.15	3	2	7.947	4	2	22.2	3	2	7.948	4	2
15	25.19	Bending Mode		8.057	3	2	25.12	Bending Mode		8.059	3	2
16	25.19	Bending Mode		8.057	3	2	25.12	Bending Mode		8.059	3	2

Table C.2: The frequencies of the cylindrical shells with 2 stiffeners at z/L=0.2 and z/L=0.25.

Mode Number	2 Stiffeners (z/L=0.2)						2 Stiffeners (z/L=0.25)					
	t/R=1e-2			t/R=1e-3			t/R=1e-2			t/R=1e-3		
	Freq. (Hz)	n	m	Freq. (Hz)	n	m	Freq. (Hz)	n	m	Freq. (Hz)	n	m
1	Rigid body motions.			Rigid body motions.			Rigid body motions.			Rigid body motions.		
2												
3												
4												
5												
6												
7	21.79	2	2	8.127	5	3	23.44	2	1	8.47	5	2(+1)
8	21.79	2	2	8.127	5	3	23.44	2	1	8.47	5	2(+1)
9	22.68	2	1	8.598	5	2(+2)	23.52	2	2	9.104	5	2(+2)
10	22.68	2	1	8.598	5	2(+2)	23.52	2	2	9.104	5	2(+2)
11	23.76	3	2(+1)	9.373	4	2(+1)	24.54	3	2(+1)	9.539	6	2(+1)
12	23.76	3	2(+1)	9.373	4	2(+1)	24.54	3	2(+1)	9.539	6	2(+1)
13	24.42	3	2(+1)	9.388	6	2(+1)	25.17	Bending Mode		9.833	6	2(+2)
14	24.42	3	2(+1)	9.388	6	2(+1)	25.17	Bending Mode		9.833	6	2(+2)
15	25.16	Bending Mode		9.598	6	2(+2)	25.55	3	2(+2)	10.03	4	2(+1)
16	25.16	Bending Mode		9.598	6	2(+2)	25.55	3	2(+2)	10.03	4	2(+1)

Table C.3: The frequencies of the cylindrical shells with 2 stiffeners at z/L=0.3 and z/L=0.4.

Mode Number	2 Stiffeners (z/L=0.3)						2 Stiffeners (z/L=0.4)					
	t/R=1e-2			t/R=1e-3			t/R=1e-2			t/R=1e-3		
	Freq. (Hz)	n	m	Freq. (Hz)	n	m	Freq. (Hz)	n	m	Freq. (Hz)	n	m
1	Rigid body motions.			Rigid body motions.			Rigid body motions.			Rigid body motions.		
2												
3												
4												
5												
6												
7	23.75	2	1	8.879	5	3	21.74	2	1	8.583	5	3
8	23.75	2	1	8.879	5	3	21.74	2	1	8.583	5	3
9	25.19	Bending Mode		9.692	6	3	24.96	3	3	9.59	6	3
10	25.19	Bending Mode		9.692	6	3	24.96	3	3	9.59	6	3
11	25.3	2	2	9.734	5	2(+2)	25.23	Bending Mode		10.3	4	3
12	25.3	2	2	9.734	5	2(+2)	25.23	Bending Mode		10.3	4	3
13	25.34	3	3	10.14	6	2(+2)	28.74	2	2	11.03	6	4
14	25.34	3	3	10.14	6	2(+2)	28.74	2	2	11.03	6	4
15	26.95	3	2(+2)	10.65	4	3	30.83	3	2(+2)	11.46	5	4
16	26.95	3	2(+2)	10.65	4	3	30.83	3	2(+2)	11.46	5	4

Table C.4: The frequencies of the cylindrical shells with 2 stiffeners at z/L=0.5 and z/L=1.

Mode Number	2 Stiffeners (z/L=0.5)						2 Stiffeners (z/L=1)					
	t/R=1e-2			t/R=1e-3			t/R=1e-2			t/R=1e-3		
	Freq. (Hz)	n	m	Freq. (Hz)	n	m	Freq. (Hz)	n	m	Freq. (Hz)	n	m
1	Rigid body motions.			Rigid body motions.			Rigid body motions.			Rigid body motions.		
2												
3												
4												
5												
6												
7	18.2	2	1	7.52	5	3	7.965	2	1	4.316	4	1
8	18.2	2	1	7.52	5	3	7.965	2	1	4.316	4	1
9	22.48	3	1(+2)	8.188	4	3	17.65	2	2	4.4	3	1
10	22.48	3	1(+2)	8.188	4	3	17.65	2	2	4.4	3	1
11	25.26	Bending Mode		9.12	6	3	18.88	3	1	5.77	2	1
12	25.26	Bending Mode		9.12	6	3	18.88	3	1	5.77	2	1
13	30.87	2	2	11.91	7	3	21.09	3	2	5.979	5	1
14	30.87	2	2	11.91	7	3	21.09	3	2	5.979	5	1
15	35.71	3	4	12	6	4	25.01	Bending Mode		7.3	5	2
16	35.71	3	4	12	6	4	25.01	Bending Mode		7.3	5	2

C.2 Results for the variation of the frequencies with the number of uniformly distributed ring stiffeners

In the tables "*n*" is the number of circumferential full waves and "*m*" is the number of longitudinal half waves.

Table C.5: The frequencies of the unstiffened and stiffened cylindrical shells (3 stiffeners).

Mode Number	Unstiffened						3 Stiffeners					
	t/R=1e-2			t/R=1e-3			t/R=1e-2			t/R=1e-3		
	Freq. (Hz)	n	m	Freq. (Hz)	n	m	Freq. (Hz)	n	m	Freq. (Hz)	n	m
1	Rigid body motions.			Rigid body motions.			Rigid body motions.			Rigid body motions.		
2												
3												
4												
5												
6												
7	7.728	2	1	2.714	3	1	17.64	2	1	7.309	5	2
8	7.728	2	1	2.714	3	1	17.64	2	1	7.309	5	2
9	17.21	2	2	3.753	4	1	17.66	2	2	7.642	4	2
10	17.21	2	2	3.753	4	1	17.66	2	2	7.642	4	2
11	18.72	3	1	4.093	2	1	21.09	3	2	8.648	5	2
12	18.72	3	1	4.093	2	1	21.09	3	2	8.648	5	2
13	20.32	3	2	5.831	5	1	23.32	3	2	9.048	6	2
14	20.32	3	2	5.831	5	1	23.32	3	2	9.048	6	2
15	25.27	Bending Mode		5.838	4	2	24.94	Bending Mode		9.624	6	2
16	25.27	Bending Mode		5.838	4	2	24.94	Bending Mode		9.624	6	2

Table C.6: The frequencies of the stiffened cylindrical shells with 5 and 7 stiffeners.

Mode Number	5 Stiffeners						7 Stiffeners					
	t/R=1e-2			t/R=1e-3			t/R=1e-2			t/R=1e-3		
	Freq. (Hz)	n	m	Freq. (Hz)	n	m	Freq. (Hz)	n	m	Freq. (Hz)	n	m
1	Rigid body motions.			Rigid body motions.			Rigid body motions.			Rigid body motions.		
2												
3												
4												
5												
6												
7	24.93	Bending Mode		13.07	6	4	24.88	Bending Mode		19.38	7	6
8	24.93	Bending Mode		13.07	6	4	24.88	Bending Mode		19.38	7	6
9	27.58	2	1	13.87	7	4	33.68	2	1	19.59	8	6
10	27.58	2	1	13.87	7	4	33.68	2	1	19.59	8	6
11	31.21	2	2	15.04	7	4	37.01	2	2	20.71	8	6
12	31.21	2	2	15.04	7	4	37.01	2	2	20.71	8	6
13	38.03	3	4	15.1	5	4	47.86	2	3	21.17	7	6
14	38.03	3	4	15.1	5	4	47.86	2	3	21.17	7	6
15	40.9	3	4	15.14	6	4	56.87	4	6	21.84	9	6
16	40.9	3	4	15.14	6	4	56.87	4	6	21.84	9	6

Table C.7: The frequencies of the stiffened cylindrical shells with 9 and 11 stiffeners.

Mode Number	9 Stiffeners						11 Stiffeners					
	t/R=1e-2			t/R=1e-3			t/R=1e-2			t/R=1e-3		
	Freq. (Hz)	n	m	Freq. (Hz)	n	m	Freq. (Hz)	n	m	Freq. (Hz)	n	m
1	Rigid body motions.			Rigid body motions.			Rigid body motions.			Rigid body motions.		
2												
3												
4												
5												
6												
7	24.81	Bending Mode		21.36	Bending Mode		24.74	Bending Mode		20.89	Bending Mode	
8	24.81	Bending Mode		21.36	Bending Mode		24.74	Bending Mode		20.89	Bending Mode	
9	38.61	2	1	25.74	8	8	42.85	2	1	32.04	9	10
10	38.61	2	1	25.74	8	8	42.85	2	1	32.04	9	10
11	41.64	2	2	25.77	9	8	45.66	2	2	32.21	10	10
12	41.64	2	2	25.77	9	8	45.66	2	2	32.21	10	10
13	51.61	2	3	26.72	9	8	54.91	2	3	32.99	10	10
14	51.61	2	3	26.72	9	8	54.91	2	3	32.99	10	10
15	62.74	Bending Mode		27.16	8	8	62.55	Bending Mode		33.15	9	10
16	62.74	Bending Mode		27.16	8	8	62.55	Bending Mode		33.15	9	10

References

[1] Norwood, C., "The Free Vibration Behaviour of Ring Stiffened Cylinders - A Critical Review of the Unclassified Literature", 1995.

[2] Markus, S., *The Mechanics of Vibrations of Cylindrical Shells*, Elsevier, 1988.

[3] Chapelle, D. and Bathe, K. J., *The Finite Element Analysis of Shells: Fundamentals*, 2nd ed., Springer Verlag, 2011.

[4] Loy, C. T.and Lam, K. Y., "Vibration of Cylindrical Shells with Ring Support", *International Journal of Mechanical Sciences* , 39, 4, 455-471, 1997.

[5] Bathe, K. J., *Finite Element Procedures*, Prentice Hall, 1996.

[6] Ugural, A. and Fenster, S., *Advanced Strength and Applied Elasticity*, 4th ed., Prentice Hall, 2009.

[7] ADINA R&D, I., *ADINA Theory and Modeling Guide*, June 2010.

[8] Bucalem, M. L. and Bathe, K. J., *The Mechanics of Solids and Structures: Hierarchical Modeling and the Finite Element Solution*, Springer Verlag, 2011.

[9] Bathe, K.J. and Dvorkin, E.N., "Four-Node Plate Bending Element Based On Mindlin/Reissner Plate Theory and A Mixed Interpolation", *International Journal for Numerical Methods in Engineering* , 21, 2, 367-383, 1985.

[10] Bathe, K. J.and Dvorkin, E. N., "A Formulation of General Shell Elements-The Use of Mixed Interpolation of Tensorial Components", *International Journal for Numerical Methods in Engineering* , 22, 3, 697-722, 1986.

[11] Bucalem, M.and Bathe, K. J., "Higher-Order MITC General Shell Elements", *International Journal for Numerical Methods in Engineering* , 36, 21, 3729-3754, 1993.

[12] Bathe, K. J., Iosilevich, A. and Chapelle, D., "Evaluation of the MITC Shell Elements", *Computers and Structures* , 75, 1, 1-30, 2000.

[13] Ajayan, P.and Zhou, O., "Applications of Carbon Nanotubes", *Carbon Nanotubes* , 391-425, 2001.

[14] Dvorkin, E. N.and Bathe, K. J., "Continuum Mechanics Based Four-Node Shell Element for General Non-Linear Analysis", *Engineering Computations* , 1, 1, 77-88, 1984.

[15] Artioli, E., Beirao Da Veiga, L., Hakula, H. and Lovadina, C., "On the Asymptotic Behaviour of Shells of Revolution in Free Vibration", *Computational Mechanics* , 44, 1, 45-60, 2009.

[16] Ventsel, E. and Krauthammer, T., *Thin Plates and Shells: Theory, Analysis and Applications*, Marcel Dekker, Inc., 2001.